IOWA STATE UNIVERSITY
Digital Repository

2016

Experimental investigation of oxygen quenching in jet fuel fluorescence for liquid-vapor discrimination

Benjamin Jordan Reuter
Iowa State University

Experimental investigation of oxygen quenching in jet fuel fluorescence for liquid-vapor discrimination

by

Benjamin Jordan Reuter

A thesis submitted to the graduate faculty

in partial fulfillment of the requirements for the degree of

MASTER OF SCIENCE

Major: Mechanical Engineering

Program of Study Committee:
Terrence Meyer, Co-Major Professor
James Michael, Co-Major Professor
Hui Hu

Iowa State University

Ames, Iowa

2016

DEDICATION

This work is dedicated to my parents. Without their endless love, support, and encouragement none of my accomplishments would have been possible. They have equipped me with the determination, intellect, and indomitable spirit to achieve success in the pursuit of my dreams. I am proud to be their son.

TABLE OF CONTENTS

LIST OF FIGURES

LIST OF TABLES

ACKNOWLEDGMENTS

First, I would like to thank God for blessing me with the opportunity to grow as a student, develop my engineering skills, and become a better man. I would also like to thank my family for their unconditional support, and for instilling in me the importance of education.

I thank my advisors Prof. Terry Meyer and Prof. James Michael, and my committee member Prof. Hui Hu for all of their guidance and patience throughout the course of this research. I owe a great deal of gratitude to the United States Air Force and Spectral Energies, LLC for allowing me to continue this research project at the Wright-Patterson Air Force Base, and I thank everyone who helped me with my research during my time working in the Air Force Research Laboratory.

Finally, I would like to say, "Thank you" to Iowa State University. Thank you for an incredible undergraduate adventure that led to a graduate experience where I was able to broaden my understanding of engineering and science, while simultaneously developing a deeper level of knowledge in a specific field. Thank you to all of the friends, fraternity brothers, classmates, and committee members that I have connected with during my time at Iowa State. You have all made a much larger positive impact on my life than I could possibly have ever imagined. I would especially like to thank Szuyin Leow for teaching me that an engineer can make a lasting impression through their emotional support and leadership in addition to their technical knowledge.

ABSTRACT

Fuel injection, vaporization, and mixing results in an extremely complex multiphase flow field that requires extensive experimental study in order to correctly characterize the behavior of combustion systems. Accurately measuring the mass fraction and volume distribution of liquid and vapor phases has been a particularly challenging task. Previous experiments have over predicted local measurements of mole fraction at the interface between regions of liquid and vapor phases. Increasing our knowledge and understanding in this area has great potential for addressing essential requirements for the improvement of combustor and engine design such as reducing emissions, increasing fuel efficiency, and boosting performance. The goal of the current work is to develop a diagnostic strategy that is able to successfully discriminate between the liquid and vapor phases. Laser-induced fluorescence is employed to perform *in situ* measurements without disturbing the underlying physics of the flow. However, the photophysics of ketones—such as acetone—and aromatic hydrocarbons that are commonly found in fuels are drastically different. A dissimilarity between these two classes of fluorescing molecules that may prove to be a key component in liquid-vapor discrimination is their response to oxygen, and the ensuing effects of collisional quenching. Experiments were performed at the Wright-Patterson Air Force Base investigating the effects of oxygen when present in the surrounding environment as well as when the fuel had been purged with various quantities of oxygen via a technique called sparging. Results are briefly discussed and recommendations for future work are presented.

CHAPTER 1

INTRODUCTION

The numerous applications of liquid sprays have made them a topic of great interest

for several decades (Lefebvre 1989). Common practical uses of sprays include, but are not

limited to: crop treatment, aerosol drug delivery, thermal management during

manufacturing processes, and fuel delivery in combustion systems for power production

(Tate 1969; Lefebvre 1989). In agriculture, sprays are used to control unwanted plant

growth such as weeds and certain types of grasses, serve as an insect deterrent, and are

also a method of distributing fertilizer. Design of agricultural spray nozzles requires

careful consideration regarding droplet diameter and velocity, operating pressure, volume

distribution pattern, orifice geometry, spray structure, and entrained air characteristics in

order to maximize the effectiveness of the crop treatment, while minimizing negative

effects such as off-target drift and plant scorching (Miller and Butler Ellis 2000; Nuyttens et

al. 2007). In the medical field, bronchodilators, pressurized metered-dose inhalers, and

similar aerosol drug delivery devices depend on the mixing of a liquid-phase medicine with

a gaseous propellant. Knowledge of the droplet size distribution and velocity field, among

other factors, is critical for efficient, localized deposition and rapid, effective clinical

response to pulmonary symptoms (Newman 2005; Dolovich and Dhand 2011). Liquid

sprays are also often utilized in manufacturing processes as a lubricant and as a means of

preventing the overheating of workpiece material. This in turn reduces the required cutting

forces and the wear on cutting or drilling tools in addition to improving the surface finish

and overall quality of the product. All of these factors allow high-speed machining, which results in increased productivity and lower manufacturing costs (Kishawy et al. 2005). The aforementioned applications are very interesting in their own right, however the focus of the work presented is dedicated to the application of sprays in combusting flows for power and propulsion systems.

Combustion is a very important topic to study. In the United States alone, nearly 80 quadrillion Btu were consumed using combustion-derived energy systems (designated by coal, crude oil, and natural gas as the energy source) in 2015. This corresponds to approximately 81% of all energy consumed in the United States during that period (Annual Energy Review 2015). An overview of energy consumption in the United States as provided by the US Department of Energy is shown in Figure 1.1
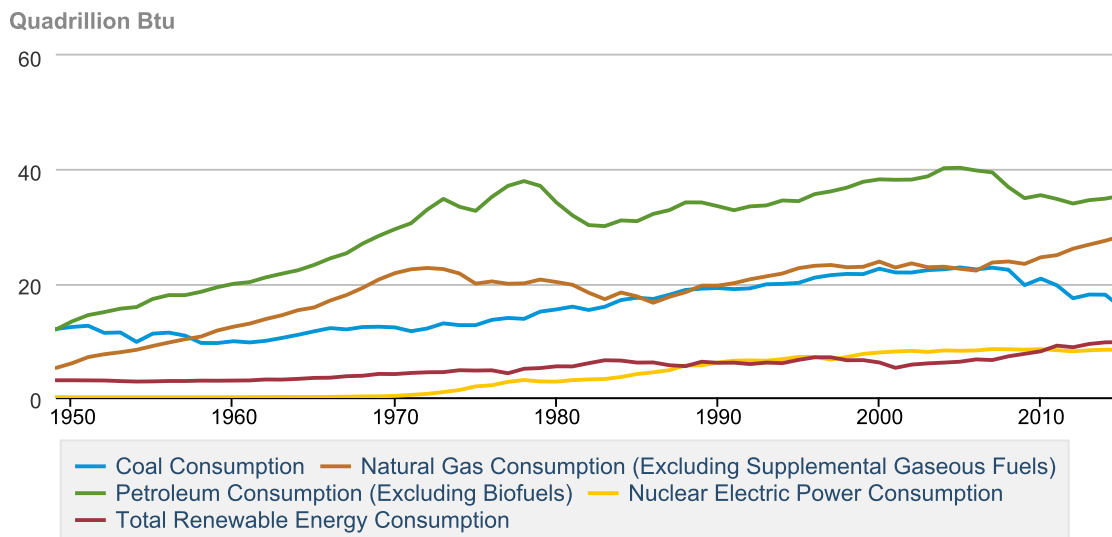
Source: U.S. Energy Information Administration

Figure 1.1: United States Primary Energy Consumption by Source (Annual Energy Review 2015)

It is clear that combustion energy is essential to our society; even so there are drawbacks to this technology—namely pollution. The thermochemical processes that generate heat and power also produce compounds that are harmful to the environment. Unburned hydrocarbons, nitrogen oxides (NO, NO_2), carbon monoxide (CO), sulfur oxides (SO_2, SO_3), and particulate matter are all unwanted products of the chemical reactions that take place during combustion (Turns 2012). A tiered system of permitted emissions has been put into effect by the Environmental Protection Agency. These regulations incentivized engine manufacturers to drastically reduce the amount of pollutants generated by combustion energy systems. A diagram showing the changes in regulations over from 1996–2015 is displayed in Figure 1.2.
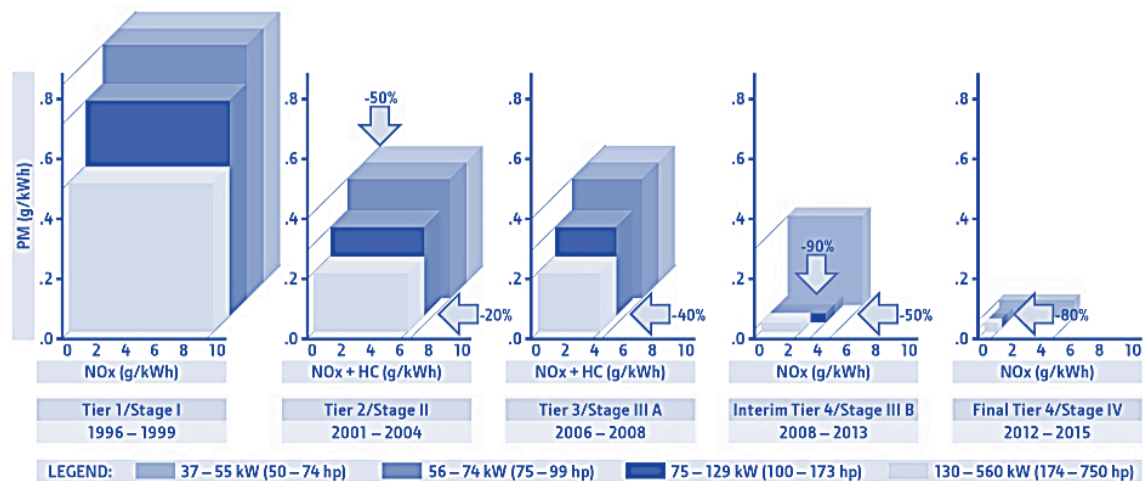
Figure 1.2: EPA and EU nonroad vehicle emissions regulations: 37-560 kW (50-750hp) (John Deere 2015)

Sophisticated aftertreatment packages have been engineered to reduce emissions for most land-based combustion systems such as internal combustion engines. Liquid sprays also play an important role in these aftertreatment packages. Urea, an ammonia-based solution, is typically injected into the exhaust of diesel engines as a method of

reducing nitrous oxide emissions. Still, these cannot be practically implemented in every situation. For instance, the strict weight constraints in the aerospace industry prohibit the use of such aftertreatment packages. Thus, there is still a strong need to decrease the amount of pollutants produced by many combustion power sources.

Combustion is the heart of the transportation industry. It is used in the vast majority of vehicles, including on- and off-road vehicles, aircraft, ships, and trains. The dominating source of fuel in the transportation industry is liquid fuels originating from petroleum. Liquid fuels are advantageous because they are abundant, easily stored and transported, and have a high energy density.

In order to unleash the chemical energy stored in liquid fuels, the liquid must first vaporize and mix with an oxidizer (usually air) prior to ignition. Two of the most common applications of liquid fuels, internal combustion engines and gas-turbine engines, introduce fuel to the combustion chamber via an atomizing injector to create particle-sized fuel droplets. However, the technology used in liquid-rocket engines injects fuel and liquid oxidizer as impinging jets. After the impinging point these jets initially form an unstable liquid sheet, which eventually breaks up into ligaments, and ultimately droplets before vaporizing. Some modern rocket engines utilize hypergolic propellants that ignite spontaneously upon contact. Because an ignition system is not necessary, these propellants are useful for missions requiring frequent engine restart, such as spacecraft maneuvering and second stage burns beyond planetary atmospheres.

Fuel injection, vaporization, and mixing results in an extremely complex multiphase flow field that requires extensive experimental study in order to correctly characterize the behavior of combustion systems. Accurately measuring the mass fraction and volume

distribution of liquid and vapor phases has been a particularly challenging task. Previous experiments have over predicted local measurements of mole fraction at the interface between regions of liquid and vapor phases (Charogiannis and Beyrau 2013). Increasing our knowledge and understanding in this area has great potential for addressing essential requirements for the improvement of combustor and engine design such as reducing emissions, increasing fuel efficiency, and boosting performance. The goal of the current work is to develop a diagnostic strategy that is able to successfully discriminate between the liquid and vapor phases.

However, obtaining information from the high-temperature, high-pressure, and highly turbulent environments that are common amongst combustion power systems requires the use of specific measurement techniques that do not disturb the nature of the phenomena. Laser diagnostics offer the ability to perform *in situ* measurements that do not interfere with the physics of multiphase flows. Several different techniques involving sophisticated technologies have been developed over the years, allowing quantitative measurements of various sprays, flows, flames, and plasmas. Even so, polydisperse sprays are prone to immense scattering, which makes it difficult to obtain accurate quantitative measurements. Other techniques, such as X-ray radiography, are not as susceptible to challenges associated with scattering. However, these techniques have their own drawbacks as well. Further discussion on alternative methods is available in **Chapter 2: Literature Review**.

The reader is presented with a review of literature that will be helpful in understanding the history and fundamentals of laser diagnostics and spray measurement techniques. The experimental facilities are described, and specific testing parameters are

defined. The behavior of the laser and imaging systems were analyzed, and calibration data is shown. A strategy for two-phase measurements is presented, and the viability of the technique is discussed. Challenges to the technique are acknowledged with recommendations for future work on the topic, and final conclusions are made.

CHAPTER 2

LITERATURE REVIEW

This chapter introduces the reader to vital concepts that are prerequisites to comprehending the current work. This information is presented in three parts: First, a short discussion provides a broad overview of alternative measurement techniques. Then, Section 2.1 describes Lorenz-Mie Theory, and Section 2.2 introduces laser-induced fluorescence and phosphorescence. The latter two sections each provide a lesson on the theory of these fundamental laser diagnostic techniques prior to a brief discussion on work done to apply these diagnostic methods to the investigation of sprays and liquid-vapor-phase measurements.

Section 2.1: Motivation

An interesting and important topic in the combustion diagnostics community is fuel-air mixture preparation. This topic is vital because it has applications to several different combustion systems, including gasoline and diesel internal combustion engines, gas-turbine engines, and rocket engines (Meyer et al. 2010). Each of these systems relies on liquid fuels to vaporize and mix with an oxidizer. These complex interactions cause difficulties when attempting to characterize the spray, especially because of light scattering in dense regions. There are numerous diagnostic techniques that have been applied to the investigation of sprays in combustion environments, but will not be discussed in great detail here. Examples of some of these include holography (Trolinger 1985), X-ray radiography (Powell et al. 2000), ballistic imaging (Linne et al. 2006), and filtered Rayleigh

scattering (Forkey et al. 1996; Allison, McManus, and Sutton 2016). In order to develop efficient, stable, and environmentally conscious combustors, detailed studies must be conducted to measure local mixture fraction for complete characterization of injecting sprays.

Section 2.2: Mie Scattering

Section 2.2.1: Light scattering theory

There are three possible responses that light can have as it interacts with any given media: absorption, scattering, and transmission. Scattering is considered to be elastic if the scattered light has the same wavelength as the light that was incident upon the scattering object. When the scattered light is either red shifted or blue shifted from the incident light, it is called inelastic scattering. Furthermore, characterization of scattering phenomena in a spray is dependent on the relationship of the wavelength of incident light with the size of the interacting particle. The interaction is characterized as Rayleigh scattering when the particle diameter is much less than the wavelength of incident light. In environments relative to power and propulsion applications—where the temperature is elevated and sprays are commonly dense—optical detection of liquid particles of this scale is difficult due to the fact that they are subject to evaporation and their scattering signals are easily eclipsed by larger particles. Because of these reasons, the complex physics associated with Rayleigh scattering will not be discussed at depth. For droplet sizes much larger than the wavelength of incident light, geometrical optics laws are appropriate. In the case where the incident wavelength and particle diameter are of the same magnitude, or the diameter is limited to a few orders of magnitude larger, Lorenz–Mie Theory is used to describe

scattering (Wriedt 2012). The relationship between particle size and incident wavelength is summarized in Table 2.1 (Meyer et al. 2010).

Table 2.1: Light scattering regimes

Particle Size to Light Wavelength Relationship	Scattering Regime
$D \ll \lambda/\pi$	Rayleigh
$D \sim \lambda/\pi$	Lorenz–Mie Theory
$D \gg \lambda/\pi$	Geometrical Optics Theory

Lorenz-Mie Theory is a solution to Maxwell's equations that calculates electromagnetic wave scattering caused by interactions with spherical particles. Mathematical details and the derivation of Lorenz-Mie Theory are available in several texts [(van de Hulst 1957; Bohren and Huffman 1983; Lock and Gouesbet 2009). The accuracy of Lorenz-Mie Theory relies on the validity of the assumption that said particles are homogeneous, isotropic, and spherical in nature (Wriedt 2012). As shown in Figure 2.1, Mie scattering has been proven to be a function of the droplet surface area (D^2) (Le Gal, Farrugia, and Greenhalgh 1999), and as a result is extremely useful in the field of spray diagnostics for particle size measurements. Lorenz-Mie Theory has been extended to a number of applications, which are discussed in Section 2.2.2.
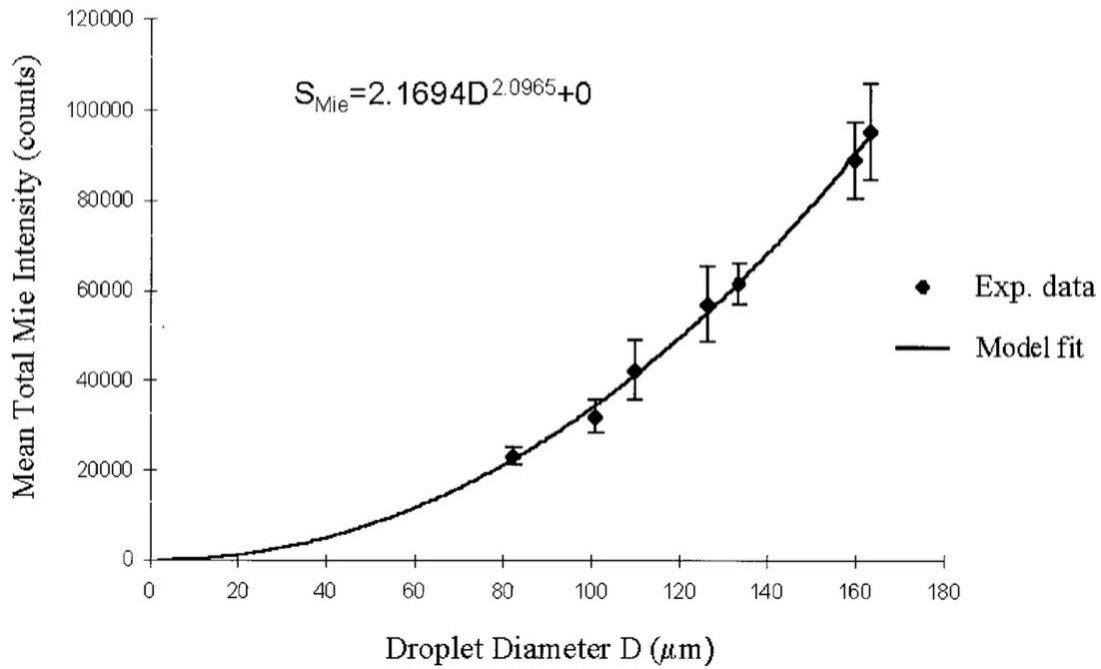
Figure 2.1: Mean total Mie scattering intensity vs. droplet diameter (Le Gal, Farrugia, and Greenhalgh 1999)

Section 2.2.2: Development of scattering diagnostic techniques

As the technology of laser diagnostics has evolved, experimentalists have implemented these techniques to their studies in more innovative ways. Typical requirements of spray measurements include the ability to measure droplet diameter over a wide range of sizes (from a few microns to a few millimeters), possessing an appropriate level of spatial resolution in order to effectively measure distribution in dense sprays, the capability of simultaneously measuring droplet velocity, and independence from incident light intensity, droplet absorption, and absolute scattering intensity (William D. Bachalo 1980).

Early droplet measurements were used to accurately determine particle sizes through the use of high-speed photomicrography (Ingebo 1957), however this technique is

limited by its small depth-of-field. This led to the use of scattered light principles as an

alternative to the aforementioned technique. However, the first implementation of light

scattering theory for polydisperse droplets—made by (Chin, Sliepcevich, and Tribus 1955a;

Chin, Sliepcevich, and Tribus 1955b)—was constrained by the particle size and its

refractive index relative to the surrounding media. (Dobbins, Crocco, and Glassman 1963)

introduced a method for measuring particles of arbitrary size and refractive index. Even

with these improvements over previous techniques, the theory of this method is

conditional on uniform illumination of all particles under investigation.

The Doppler effect was first used to make fluid flow measurements in the mid-

1960s with a technique called laser Doppler velocimetry (LDV) (Yeh and Cummins 1964;

Foreman, George, and Lewis 1965). An identical optical arrangement to LDV was used in

the development of phase-Doppler interferometry (PDI) (Farmer 1972). This setup,

illustrated in Figure 2.2, observed the interference fringe pattern of particles as they passed

through a set of crossed laser beams to measure particle size, number density, and velocity.
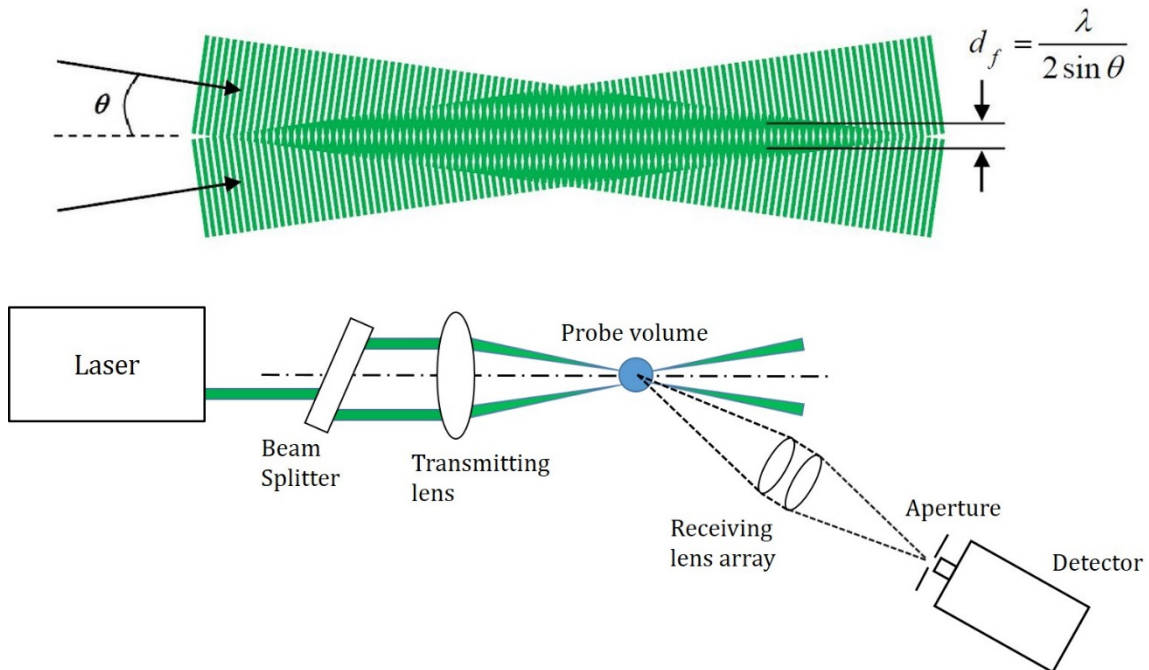
Figure 2.2: Top: Interference fringe pattern with a spacing of d_f (Meyer et al. 2010). Bottom: Standard optical arrangement for PDI measurements. Adapted from (Farmer 1972).

The overlapping region of the two planar monochromatic waves is defined as the *probe volume*. As a particle moves through the probe volume, it creates an oscillatory signal commonly referred to as the Doppler burst signal. Particle sizing and velocity information can be extracted from this Doppler burst signal, with experimental validation of droplet diameter accurate from 5 μm to 2.5 mm (William D. Bachalo 1980).

Improvements to this technique evolved into the development of the phase-Doppler particle analyzer (PDPA) (W. D. Bachalo and Houser 1984), which has become an established instrument for measuring spray dynamics (Meyer et al. 2010). PDPA is an improvement upon the technology used in LDV because it accounts for reduced fringe visibility caused by variations in relative beam intensity, polarization, and coherence. This improvement is important because fringe visibility is likely decreased in a spray

environment because of beam attenuation from larger droplets (W. D. Bachalo and Houser 1984).

A direct application of Lorenz-Mie Theory and laser-induced fluorescence is laser sheet dropsizing (LSD). LSD is a spray diagnostic technique where instantaneous or time-averaged planar images of Sauter Mean Diameter (SMD) are generated by relating Mie scattering and LIF. The SMD of a spray is defined as the diameter of a droplet with the same volume to surface area ratio as the total volume to the total surface area of all of the drops in a spray, and is commonly denoted as D_{32} (Schick 1997). Having improved spatial and temporal resolution, LSD offers more information at a faster rate, and is especially useful when investigating dense regions of sprays (Le Gal, Farrugia, and Greenhalgh 1999).

Similar to the diameter squared dependence of Mie scattering mentioned above, fluorescence has been shown to be a function of droplet volume (D^3) (Le Gal, Farrugia, and Greenhalgh 1999). Carefully calibrated experimental data validating this dependence is shown in Figure 2.3.
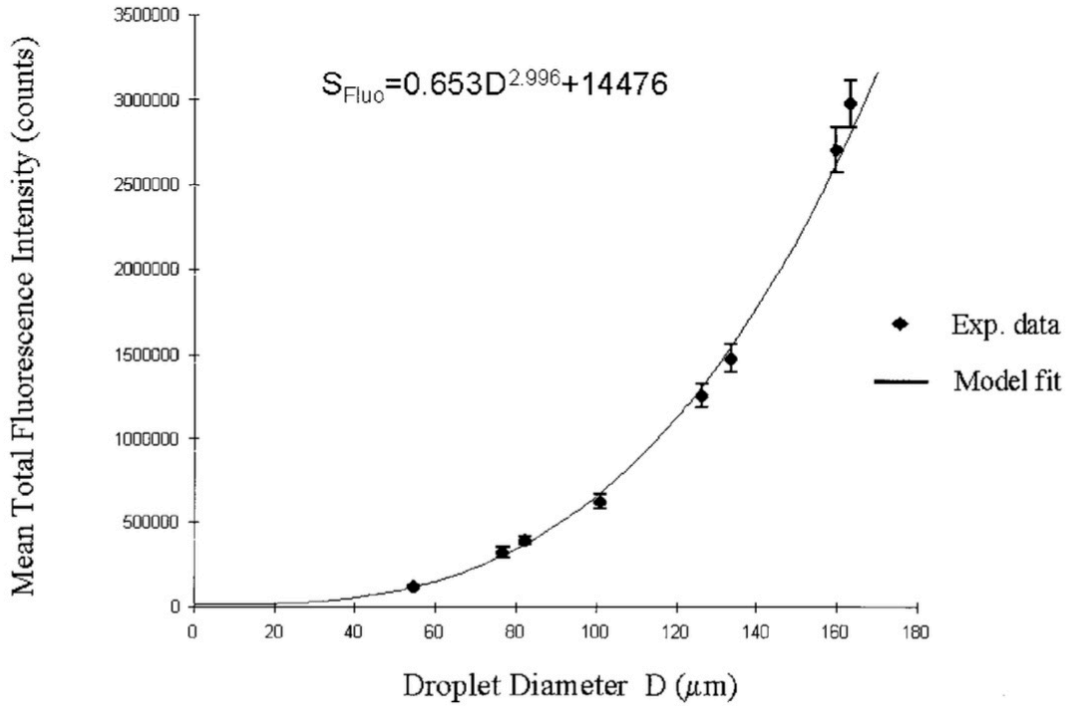
Figure 2.3: Mean total LIF intensity vs. droplet diameter (Le Gal, Farrugia, and Greenhalgh 1999)

Signal intensity equations used in LSD for Mie scattering and LIF have been written as

$$S_{Mie} = C_{Mie}I_0 e^{-kx} Q_{sca} \int_0^\infty D^2 \frac{dn}{dD} dD$$

and

$$S_{LIF} = C_{LIF}I_0 e^{-kx} \int_0^\infty D^3 \frac{dn}{dD} dD$$

C_{Mie} and C_{LIF} are coefficients that are determined by the arrangement of the optics and detection system, I_0 is the intensity of the incident laser light, k accounts for the effects of attenuation, x represents the distance traveled by the laser beam, Q_{sca} is a parameter related to the signal collection solid angle, D is the droplet diameter, and dn is the droplet number density between D and $D+dD$.

Because SMD represents the relationship between volume and surface area of a spray, and fluorescence and scattering are dependent on these two characteristics, it can clearly be seen that SMD can be calculated by dividing the LIF intensity by the Mie scattering signal intensity:

$$\frac{S_{LIF}}{S_{Mie}} = \frac{C_{LIF}}{C_{Mie}Q_{sca}} \frac{\int_0^\infty D^3 dn}{\int_0^\infty D^2 dn} = \frac{D_{32}}{C}.$$

Section 2.3: Laser-induced Fluorescence and Phosphorescence

Section 2.3.1: Photophysics of laser-induced fluorescence & phosphorescence

Laser-induced fluorescence (LIF) is a powerful and well-established diagnostic technique that has been studied in great detail. Here, a brief fundamental discussion is presented for the reader. Further information on LIF theory and its applications is available in numerous references (Lucht 1987; Eckbreth 1996; Schulz and Sick 2005).

Laser-induced fluorescence is the spontaneous emission of a photon from a molecule or atom at an elevated quantum state following excitation via laser irradiation. This emission process is expressed by

$$M^* \rightarrow M + h\nu.$$

where M is the molecule and the excited state is distinguished by the superscript *. The photon emission term is the product of Planck's constant, h, and the frequency, ν.

The total spin and degree of excitation characterizes the quantum (or electronic) state of a molecule. When no electrons are excited and the total spin, S, is equal to zero the molecule is considered to be in its ground state. Each electron carries a spin of S=1/2, and is paired with another electron of anti-parallel spin in the ground state. The event where a

single electron is excited results in two unpaired electrons. The unpaired electrons may be anti-parallel and the total spin of the molecule remains zero. In this case, where the molecule is excited, but S=0, the molecule is said to be in the singlet (S) state. However, when a molecule is excited and the resulting unpaired electrons are parallel, the total spin is equal to one and the molecule is in the triplet (T) state. The degree of excitation increases with energy and is denoted by subscripts. The ground state is always expressed by S_0. The population of the molecular orbitals and the corresponding relative energy levels of the quantum states for a ketone group are shown in Figure 2.4 (Schulz and Sick 2005).
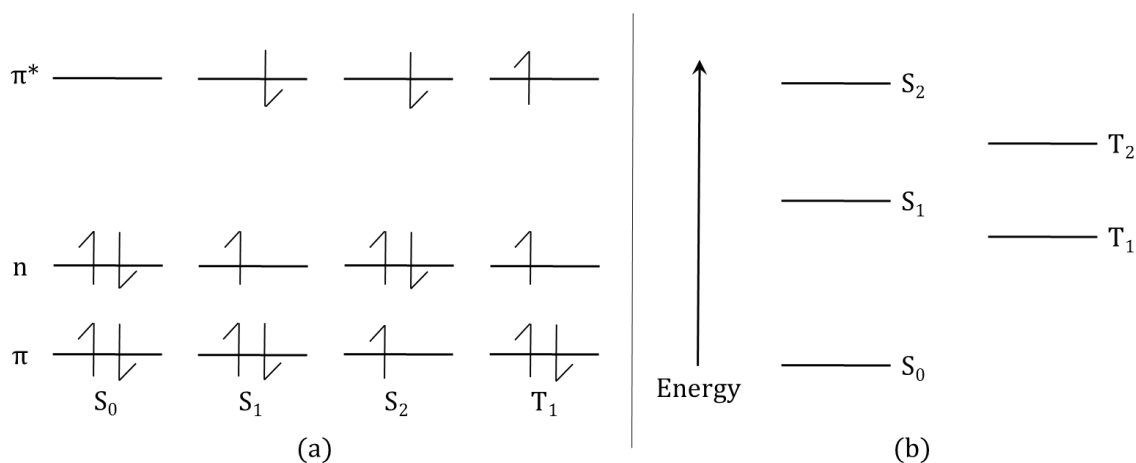
Figure 2.4: Quantum states of a ketone molecule. (a) The population of molecular orbitals shown for indicated excited states. (b) Energy levels associated with each state. Adapted from (Schulz and Sick 2005).

Once the laser has excited the molecule to a higher energy state, there are several mechanisms by which the molecule may decay back to its ground electronic state. These include spontaneous emission (fluorescence and phosphorescence), intersystem crossing where the spin of the electron is reversed, internal conversion which is a radiationless transition where the spin is conserved, vibrational relaxation, and collisional quenching

caused by physical interactions with other molecules (Tran, Kochar, and Seitzman 2005).

These processes are conveniently illustrated in the Jablonski diagram in Figure 2.5.
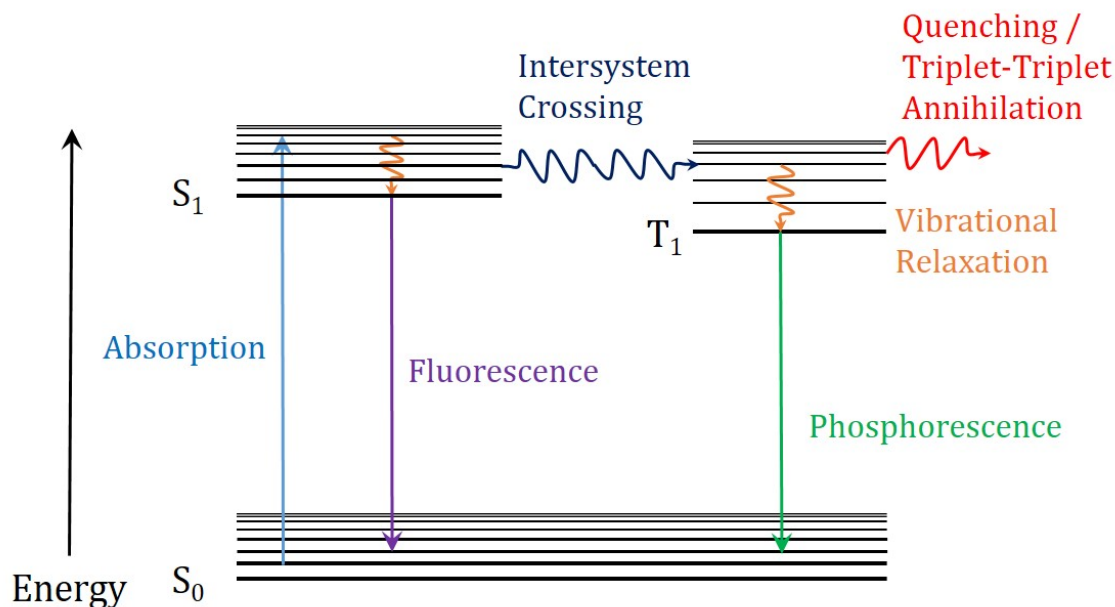
Figure 2.5: Jablonski diagram depicting excitation and relaxation mechanisms. Radiative processes are illustrated with straight lines, and non-radiative processes with wavy lines. Adapted from (Charogiannis and Beyrau 2013).

Fluorescence is the radiative de-excitation process of spontaneous emission from the singlet state. This $S_1 \rightarrow S_0$ transition has been shown to have short lifetimes, typically on the order of 1–100 ns (Lozano 1992; J. M. Seitzman and Hanson 1993). The phenomenon of spontaneous emission from the triplet state is called phosphorescence and has a much longer lifetime than fluorescence. This may be attributed to inefficient intersystem crossing from triplet states to the ground state due to large differences in energy (Schulz and Sick 2005).

A simple first-order differential equation is used to describe the rate at which an excited molecule, M^*, relaxes to its ground state via fluorescence,

$$-\frac{d}{dt}[M^*] = (k_{LIF} + k_{ic} + k_{isc})[M^*].$$

This equation accounts for the non-radiative processes of internal conversion and intersystem crossing—k_{ic} and k_{isc}, respectively—and k_{LIF} is the rate of spontaneous fluorescence emission. Solving the differential yields the exponential decay:

$$[M^*] = [M^*]_0 e^{-k_{tot}t}$$

where $[M^*]_0$ is the initial concentration of the excited molecule and k_{tot} is the sum of all depopulation processes. Therefore, the effective fluorescence lifetime is dependent on the rates of each of the depopulation mechanisms. The inverse relation is described by

$$\tau_{eff} = \frac{1}{k_{tot}}.$$

The efficiency by which excited molecules emit a photon to produce fluorescence is measured by the fluorescence quantum yield. The fluorescence quantum yield can be easily conceptualized as the fraction of molecules that are depopulated from their excited state by producing fluorescence relative to the total number of molecules that decay back to the ground state without emitting fluorescence. This concept is expressed mathematically by the equation,

$$\phi_{LIF} = \frac{\tilde{k}_{LIF}}{\tilde{k}_{tot}} = \frac{\tau_{eff}}{\tau_{rad}}.$$

The tilde above the middle terms denotes a rate coefficient. These terms are related, but distinctively different than rate of energy transfer terms such as k_{LIF} and k_{tot}. A rate coefficient represents its respective rate of energy transfer when multiplied by the appropriate number density term, n. This notation is important when considering the effects of collisional quenching.

So far in the discussion on the kinetics of photo-physical processes, the only non-radiative deactivation processes that have been considered are internal conversion and

intersystem crossing. Now that a fundamental knowledge of the role of depopulation mechanisms has been established, it is convenient to expand on the role of collisional quenching.

Collisional quenching involves the de-excitation of molecules through random inter-molecular collisions. Transfer of energy may occur when an excited molecule collides with another excited molecule or with other molecules in the environment. Oxygen quenching is a topic of special interest and will be discussed later in further detail. Let us revisit the fluorescence quantum yield expression, but now consider the effects of collisional quenching in our evaluation. The expression becomes

$$\phi_{LIF} = \frac{k_{LIF}}{k_{tot} + \tilde{k}_q n_q}.$$

Notice that the quantum yield responds inversely to increases or decreases in the number density of the quenching species, n_q. The influence of quenching on fluorescence signal intensity is expressed by

$$\frac{S_{LIF}^0}{S_{LIF}} = \frac{k_{LIF}}{k_{tot}} \frac{k_{tot} + \tilde{k}_q n_q}{k_{LIF}} = 1 + \frac{\tilde{k}_q}{k_{LIF}} n_q,$$

where S_{LIF}^0 denotes the fluorescence signal intensity in a collisionless environment. S_{LIF} is the fluorescence signal intensity as detected by the observation system and is defined as

$$S_{LIF} = \frac{E}{h\nu} V n_{LIF} \sigma_{abs} \phi_{LIF} \eta \,\Omega/4\pi.$$

where $E/h\nu$ is the photon flux, n_{LIF} is the number density of the fluorescing species that have the absorption cross-section, σ_{abs}, within the probed volume, V. The detection efficiency and solid angle observed by the detector are represented by η and $\Omega/4\pi$. As before, ϕ_{LIF} is the fluorescence quantum yield. The Stern–Volmer coefficient indicates the

significance of collisional quenching in fluorescence measurements and can be used to compare experimental observations with the ideal situation where collisional quenching effects are absent. The Stern–Volmer coefficient is expressed mathematically as

$$k_{SV} = \frac{\tilde{k}_q}{k_{tot}} = \tilde{k}_q \tau_{eff}.$$

There exists an additional depopulation mechanism specific to the triplet state of a molecule that reduces the quantum yield of phosphorescence. This mechanism is called triplet–triplet annihilation and consists of the assimilation of energy by a molecule in the triplet state as another triplet state molecule decays non-radiatively (Charogiannis and Beyrau 2013).

Empirical evidence has proven that fluorescence and phosphorescence lifetimes and signal intensities are affected by environmental conditions such as temperature, pressure, and bath gas composition (Greenblatt, Ruhman, and Haas 1984; Mark C. Thurber et al. 1998; M. C. Thurber and Hanson 1999; Charogiannis and Beyrau 2013). Dependencies on temperature and pressure are expressed within the fluorescence signal intensity equation. The number density of the fluorescing species, n_{LIF}, and the quantum yield, ϕ_{LIF}, are direct functions of temperature and pressure, while the absorption cross-section, σ_{abs}, is a dependent on temperature.

At increased pressure, acetone emission has been observed to shift from a decay with a distinct short-lifetime component and a second component with a much longer lifetime, to exhibiting two longer-lived decay components (Greenblatt, Ruhman, and Haas 1984; Copeland and Crosley 1985). Under atmospheric conditions, an excited acetone molecule in the S_1 state rapidly transitions to a mixed singlet-triplet state via an intramolecular dephasing process before experiencing intersystem crossing to the T_1 state.

At elevated pressure, the mixed singlet-triplet state is swiftly extinguished by collisional quenching (Mark C. Thurber et al. 1998). The composition of the bath gas also plays an important role in the effect of pressure on emission. For example, the fluorescence quantum yield of acetone and 3-pentanone was shown to increase with pressure in a nitrogen environment, did not change with pressure in air, and showed an inverse relationship to pressure when surrounded by oxygen (Grossmann et al. 1996; Schulz and Sick 2005).

Fluorescence and phosphorescence lifetimes of liquid acetone have also been shown to be wavelength-dependent. Returning to the fluorescence signal intensity equation, σ_{abs} and ϕ_{LIF} are dependent on the excitation wavelength in addition to temperature and pressure. Further observations showed the phosphorescence lifetime to be a function of both the excitation and detection wavelengths (Mark C. Thurber et al. 1998; M. C. Thurber and Hanson 1999; Tran, Kochar, and Seitzman 2005). Notice that the fluorescence quantum yield has been shown to be dependent on temperature, pressure, and excitation wavelength. In fact, the quantum yield accounts for all effects that hinder fluorescence. An interesting factor that influences the quantum yield is the composition of the surrounding environment, or bath gas. One specific effect that must be investigated is collisional quenching of an excited species with neighboring molecular oxygen, and how this mechanism behaves differently for various classes of fluorescing molecules.

Much of the work documented in the literature has been investigating laser-induced fluorescence and phosphorescence of acetone, which is an aliphatic ketone. Aliphatic ketones have been studied extensively and their photophysical properties are well understood. For these reasons, they provide an excellent view into the information

available once the photophysical behavior of a molecule has been completely characterized. For instance, measurements of species concentrations can be extended to measure the temperature and air-fuel ratio (Schulz and Sick 2005).

However, the properties of aliphatic ketones are drastically different than those of aromatic compounds commonly found in fuel molecules. As can be seen in Figure 2.6, the quantum yield of a ketone actually increases with pressure, even when oxygen is present in the bath gas.
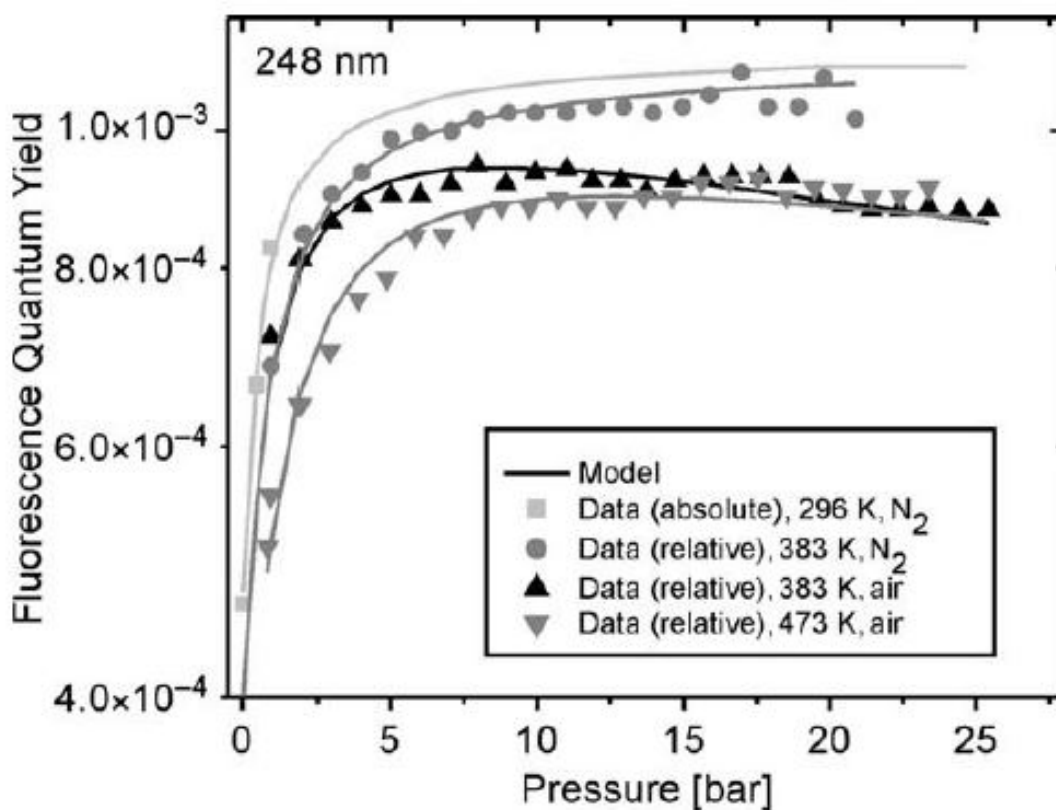

Figure 2.6: Effects of increasing pressure on fluorescence quantum yield for 3-pentanone in various environmental conditions (Schulz and Sick 2005).

This is because pressures above atmospheric conditions cause an increase in vibrational relaxation to a lower state, and these lower energy states have a longer lifetime. However,

this behavior is only observed up to a certain point. After a specific pressure threshold the effects of quenching slowly start to take over the response of the quantum yield. It should be noted that oxygen quenching is still present in ketones, and increased signals were observed because of the increased pressure. Empirical evidence has shown effects of oxygen quenching at standard pressure conditions (Charogiannis and Beyrau 2013).

Aromatic hydrocarbons have a different response. They typically produce a high fluorescence quantum yield and are effectively quenched by oxygen. Toluene and naphthalene are two commonly used aromatic hydrocarbons. The effects of increasing partial pressure of oxygen on fluorescence signal for toluene are shown in Figure 2.7. Although, further experimentation is necessary to fully characterize this class of fluorescing molecules (Schulz and Sick 2005).
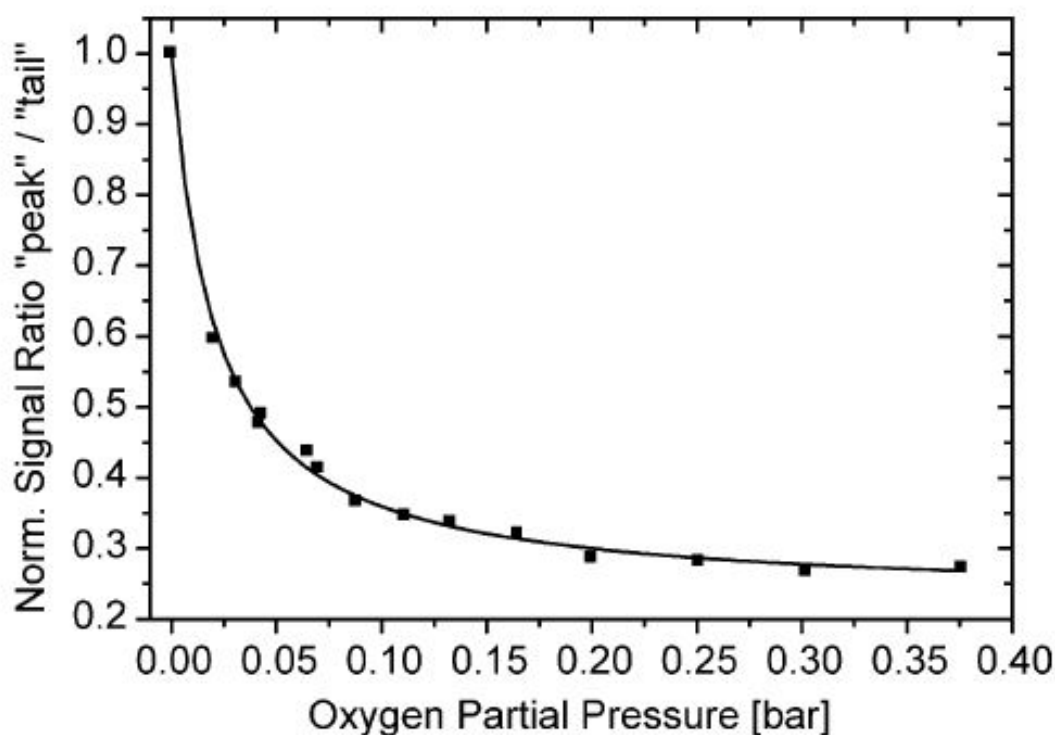

Figure 2.7: Effects of increasing partial pressure of oxygen on fluorescence signal for toluene (Schulz and Sick 2005).

Section 2.3.2: Applications of laser-induced fluorescence & phosphorescence

Laser-induced fluorescence is commonly employed in combustion and diagnostics

communities. This technique is well established in a wide breadth of applications and may

be used to investigate non-reacting flows, flames, and even plasmas. As is the nature of all

nonintrusive techniques, LIF has the strong advantage of obtaining *in situ* information

without disturbing chemical or physical processes such as reaction rates and flow

dynamics. LIF possesses the capability to measure species concentration, which requires a

high level of sensitivity and spatial resolution (Lucht 1987). In combustion environments,

LIF has been used to measure pollutant species such as CO, NO, NO_2, and SO_2 which have

hazardous environmental effects, metallic species such as Na, K, and V which can cause

corrosion and fouling in combustion systems, and free radical species such as H, O, and OH.

Concentration measurements of these transient free radicals are of special interest because

of their role in flame ignition and stability, reaction kinetics, and the formation of

pollutants. Because OH is typically present in high concentrations, shows strong signal for

multiple flame conditions, and has a thoroughly investigated spectrum, it is the ideal

species for flame temperature measurements (Lucht 1987).

Concurrent imaging of liquid- and vapor-phase mass distribution (mixture fraction)

in sprays is currently a topic of special interest for the improvement of modern combustion

systems. Knowledge to be gained from well-developed quantitative measurements has

high potential to result in improved environmental impact, performance, efficiency, and

flame stability while reducing combustor size and fatigue on the system for increased

lifetimes. Research performed by Seitzman and co-workers (Ritchie and Seitzman 2002; J.

Seitzman and Ritchie 2004; Tran, Kochar, and Seitzman 2005) focused on the specific

challenge of improving measurement strategies of mixture fraction in two-phase sprays.

One approach exploited the difference in lifetime between fluorescence and

phosphorescence of an acetone spray in order to separate the signals between the two

emission mechanisms. Another strategy, detailed by (Tran, Kochar, and Seitzman 2005),

utilized two lasers to excite at wavelengths of 266 nm and 285 nm to characterize the

photophysical response of liquid acetone. This work was a thorough spectrally and

temporally resolved study of the emissive properties of liquid acetone, however it did not

yield quantitative measurements of mixture fraction.

Simultaneous imaging of fluorescence, phosphorescence, and Mie scattering has

shown promise for achieving accurate measurements of multi-phase mass distribution

(Kiel et al. 2009). Theoretically, Mie scattering could be subtracted from fluorescence

measurements in order to separate the liquid-phase signal from the signal measured from

the vapor phase. This is based on the observation that Mie scattering is only sensitive to

the liquid phase in a spray, while laser-induced fluorescence is sensitive to both the liquid

and vapor phases of a spray. Unfortunately, because scattering is proportional to droplet

diameter squared, whereas the absorption and emission processes of laser-induced

fluorescence and laser-induced phosphorescence are proportional to diameter cubed, this

method is subject to significant error in polydisperse sprays (Berrocal et al. 2008). Luckily,

phosphorescence is easily quenched by oxygen in the vapor phase in addition to displaying

proportionality to droplet volume, so it offers an attractive alternative to Mie scattering for

subtracting from fluorescence measurements for phase separation. Experimental results

have shown that this technique provides the capability to perform image subtractions on a

droplet-by-droplet basis, although rescattering was still a significant concern in data processing (Kiel et al. 2009).

A significant challenge to measuring multi-phase images with laser-induced fluorescence is the effect of halation resulting from the large intensity disparity between the liquid and vapor phases (Charogiannis and Beyrau 2013). This effect often causes immense overprediction of vapor mole fraction in the region surrounding liquid structures. Conversely, phosphorescence imaging was tested and was able to accurately locate the liquid-vapor interface in a monodisperse stream of acetone droplets. However, the technique demonstrated in this work is only successful in the absence of oxygen, since the phosphorescence vapor phase is entirely quenched by even trace quantities of oxygen. Data demonstrating this important concept can be visualized in Figure 2.8 (Charogiannis and Beyrau 2013).
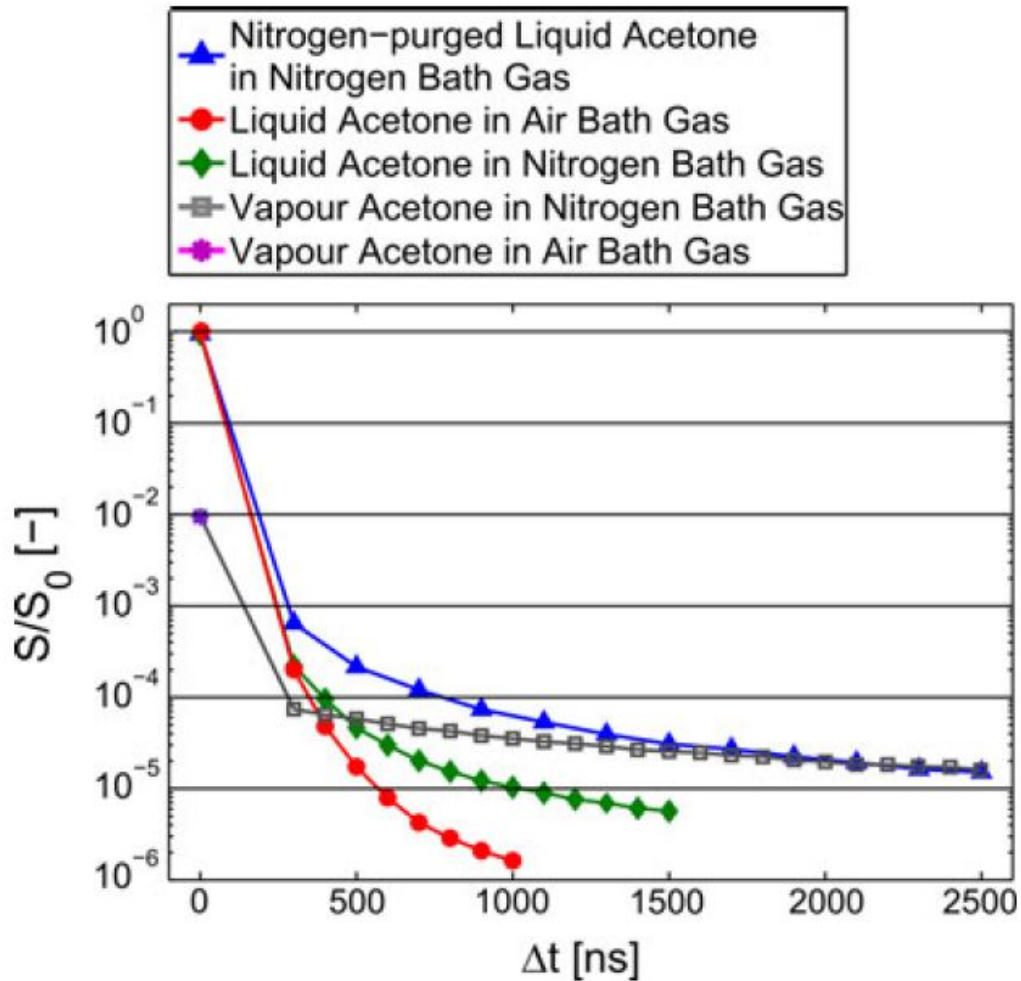
Figure 2.8: Effects of environmental composition on acetone emission (Charogiannis and Beyrau 2013).

Because of this quenching effect, the procedure required in this type of experiment

involved purging the liquid with nitrogen in order to remove dissolved oxygen within the

liquid. The process of purging the liquid phase of a fuel with a desired gas will be a

common theme throughout this paper, and will be referred to as sparging. Sparging with

nitrogen has been observed to increase signal intensity and lifetime by reducing the effects

of oxygen quenching (Charogiannis and Beyrau 2013).

CHAPTER 3

EXPERIMENTAL METHODS

The focus of this chapter is to provide a description of the experimental configuration and the behavior of the equipment used in the measurements. The chapter begins by identifying the contributing components of the entire experimental setup. Detailed discussions on the laser system, optical response of the cameras, and the testing apparatus are provided for the reader.

Section 3.1: Experimental Configuration

Section 3.1.1: Laser system

A Continuum Powerlite 8010 Nd:YAG laser was used as the excitation source throughout the entirety of the study. This system is a solid-state laser that uses a neodymium-doped yttrium aluminum garnet (Nd:$Y_3Al_5O_{12}$) crystal as its lasing medium. Typically, an Nd:YAG crystalline rod is pumped by flashlamps to emit light at a fundamental wavelength of 1064nm. In order to increase peak power, a Q-switch is employed to produce a pulsed output beam. Initially, the Q-switch is set to allow energy to build within the optical cavity as the flashlamps pump the gain medium. Eventually, the cavity will reach a level of maximum population inversion where the majority of molecules in the gain medium are in an excited quantum state. At this point, the Q-switch releases light feedback to depopulate the excited neodymium gain medium and the resulting output is a Gaussian pulse in the infrared at 1064nm.

The flashlamps of the Nd:YAG laser were triggered externally at a 10 Hz repetition rate via a method called *Direct Access Triggering* (DAT). A few additional pieces of equipment were required to use this method of triggering, including: BNC cables, a 5V dc power supply, a 9-pin male "D" style connector, and a TTL trigger circuit. A digital delay generator (Stanford Research Systems DG645) was used as the TTL trigger circuit in this setup, and was also used to trigger the PI cameras. Combining these two necessary functions into a single piece of equipment added ease of operability during data collection. Switching the delay generator from an internal triggering mode (laser firing) to an external triggering mode (laser no longer firing) also prevented the triggering signal from communicating with the cameras. Because separate computers were controlling the PI cameras, blocking the trigger signal removed the need for operators to provide the recording input to each of the PI cameras at exactly the same instant. The recording input could be applied to each camera with undefined relative timing, and the cameras would not record any data until the delay generator was switched back to internal triggering mode and the triggering signal was released to the cameras.

Another advantage of the DAT method of externally triggering the laser is that it results in a reduced amount of electronic jitter present in the system. The Continuum Powerlite 8000 Operation and Maintenance Manual claims that this method of triggering yields the lowest possible jitter of ~1ns. It was important to minimize the jitter in order to ensure that both PI cameras were observing the same laser pulse, and that the intensity of scattering, fluorescence, and phosphorescence did not change as a result of variable timing of the laser pulse with respect to the camera exposure.

The Continuum laser used in the following experiments included a Type II nonlinear doubling crystal within the optical head that was used for second harmonic generation. This crystal doubled the frequency of the laser pulse, reducing the wavelength by a factor of 2 from 1064 to 532nm, and approximately doubled its energy. After leaving the optical head, the beam was then directed to an external harmonic generator (Inrad Optics Autotracker III), which repeated the process described previously for a final wavelength in the ultraviolet of 266nm. The laser pulse duration was approximately 10ns with a peak energy level of approximately 35mJ/pulse.

Section 3.1.2: Optical arrangement

This subsection highlights the components of the optical train along the beam path as it propagates toward the measurement volume, and introduces the detectors that were used throughout the study.

Once the beam exited the optical head, it passed through a wave plate and polarizer. The wave plate was fixed in a rotating mount, providing the ability to quickly perform fine adjustment of the beam energy at any moment during experimentation. The polarizing film safely rejected the horizontally polarized infrared light within the pulse into a beam dump as it exited the optical head. A series of prisms within a spectrometer adjacent to the external harmonic generator yielded a similar result for separating green (532nm) light from the UV (266nm). Once the second and fourth harmonics of Nd:YAG were separated, the 266nm beam proceeded toward the measurement volume. A series of mirrors configured in a periscope array directed the laser beam to the measurement volume from above. The experimental configuration is shown in Figure 3.1.
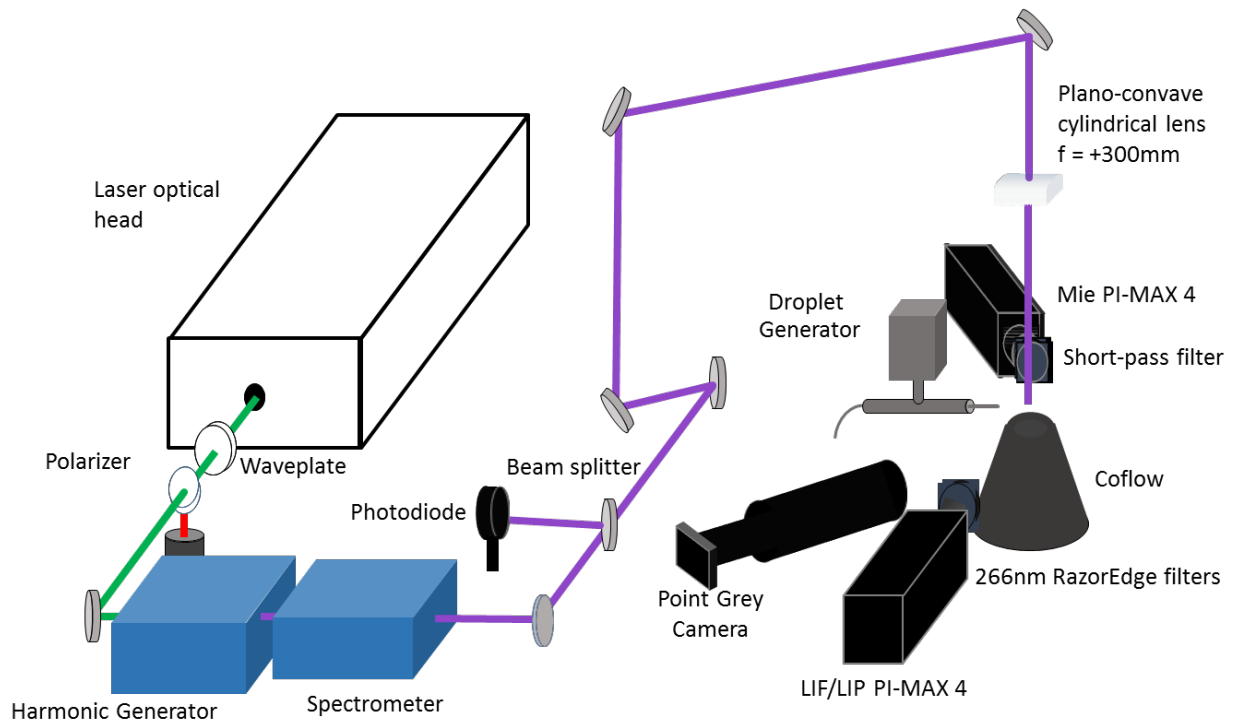
Figure 3.1: Experimental configuration.

In typical planar laser measurements, two different optical components are used to shape the beam into a thin sheet. The first component is a plano-convex, spherical lens of a specified focal length. This optic converges the beam to a point at its focus. Then, the second optic—a plano-concave, cylindrical lens—causes the beam to diverge in a single direction to create the aforementioned laser sheet. However, due to spatial constraints, only a single, UV fused silica, plano-convex, cylindrical lens was used for two-dimensional measurements in this study.

Three cameras were used throughout the study. The first camera, a Point Grey Chameleon 2.0 with a microscope objective, used shadowgraphy to measure droplet diameter. Shadowgraphy involved backlighting the measurement volume with white light. A representative image of this method is shown in Figure 3.2.
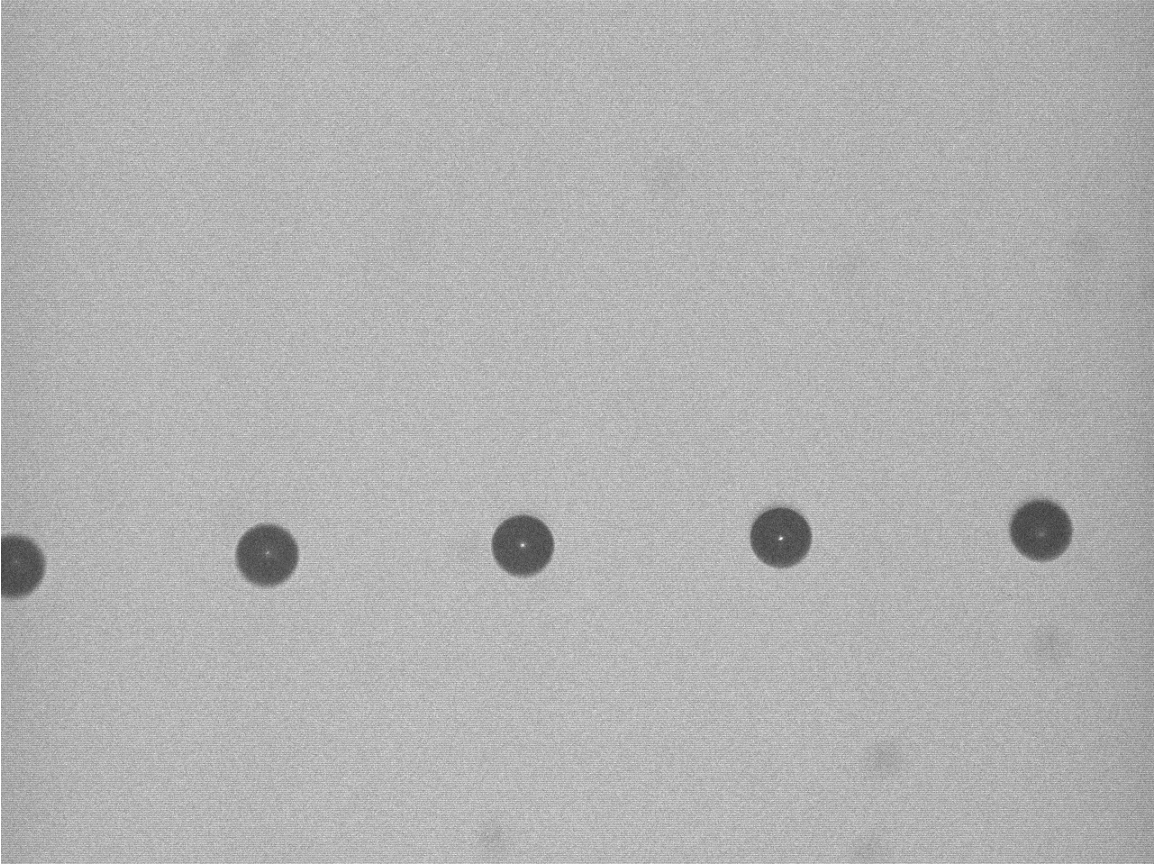
Figure 3.2: Point Grey shadowgraphy image of O₂-sparged Jet-A in a heated nitrogen cross flow. In this image the orifice diameter was 80μm and the reservoir pressure was 48 mbar.

The other two cameras were Princeton Instruments PI-MAX 4 intensified charge-coupled device (ICCD) cameras that were used to measure planar laser-induced fluorescence and phosphorescence (PLIF and PLIP), and Mie scattering, respectfully. The resolution of each of the three cameras was measured using a United States Air Force reference test chart. The resolution of the Point Grey camera was 3.7μm per pixel. The resolution values that were measured of the Mie scattering and LIF/LIP PI cameras were 49μm per pixel and 44μm per pixel, respectively. In order to capture the scattering and emission at short wavelengths, Cerco UV lenses were coupled to the PI cameras. In front of the PLIF/PLIP camera were two Semrock RazorEdge 266nm filters that blocked any light with a wavelength of 266nm or less to reduce signal from elastically scattered laser light.

An opposing strategy was used with the PI camera intended to collect Mie scattering. For

this camera, a low-pass filter was placed in front of the lens to ensure that only scattered

laser light at 266nm would be measured. Neutral density (ND) filters of varying optical

density (OD) manufactured by Edmund Optics were used when appropriate in various

experiments. Because of limited space around the measurement volume, and an undesired

reflective effect observed in the PI cameras, only one camera—the PLIF/PLIP PI-MAX 4—

was positioned orthogonally to the measurement volume. The other two cameras recorded

information from slight angles, and the images were calibrated using a United States Air

Force reference test chart as well as a Thorlabs dot chart with 1mm spacing. The

arrangement of cameras around the measurement volume can be seen in Figure 3.3.
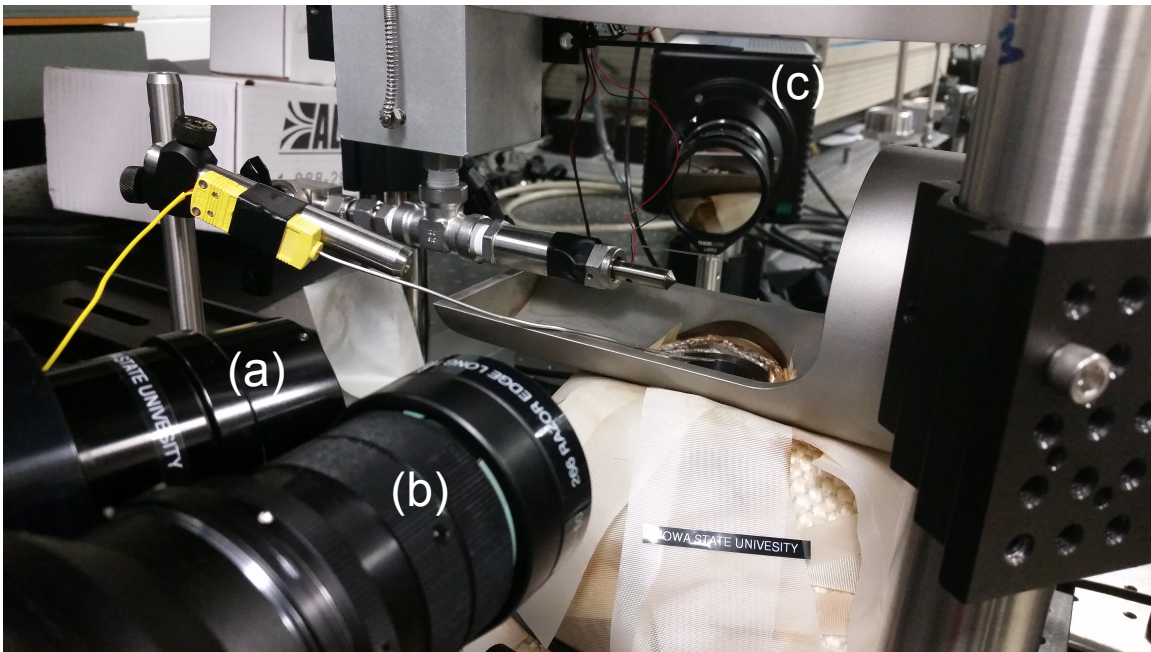

Figure 3.3: Arrangement of cameras around measurement volume. (a) Point Grey camera. (b) LIF/LIP PI-MAX 4 camera. (c) Mie scattering PI-MAX 4 camera.

Section 3.1.3: Beam characterization

The interaction of the laser beam with the measurement volume is an extremely critical event in all laser diagnostics investigations. In order for diagnostic studies to yield accurate conclusions, a thorough understanding of this interaction and how it is observed must be documented. Essential aspects that contribute to this interaction include the profile of the laser beam and the amount of energy in each laser pulse. The objective of this section is to detail how each of these essential aspects were accounted for during experimentation and data processing.

Spatial constraints once again required a creative arrangement to complete the measurement. The sheet-forming, plano-convex, cylindrical lens was temporarily removed from its mount above the measurement volume and placed in the path of the beam immediately following the beam splitter that will be discussed in Section 3.1.3. A beam profiler with a UV converter mapped the distribution of energy along the cross-sectional area of the beam using the software package BeamGage by Ophir Photonics. The beam profiler was mounted on a translation stage so that data may be collected over a range of distances from the lens. An image of the beam profile at a distance of 320mm from the lens is shown below in Figure 3.4.
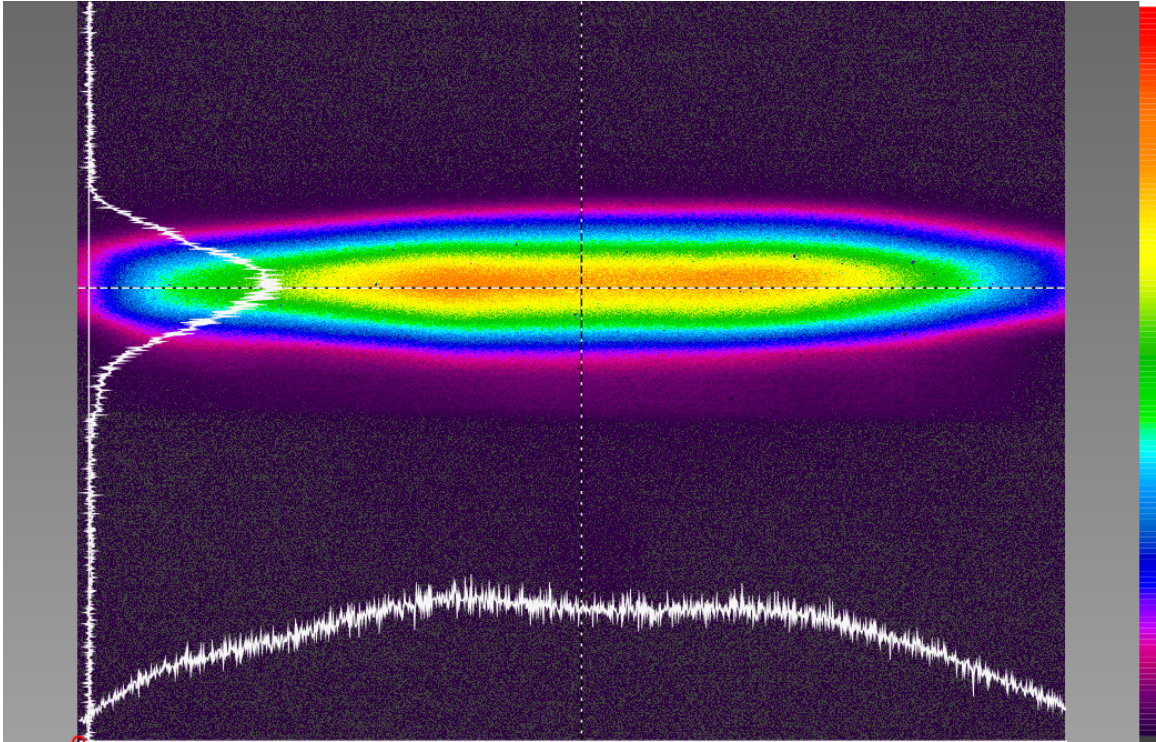
Figure 3.4: Beam profile of 300mm focal-length plano-convex cylindrical lens at 320mm.

The full-width at half-maximum (FWHM) of the Gaussian beam is an expression that is commonly used to characterize the beam profile in diagnostic studies. It is defined as the width of the Gaussian distribution at the height that is equal to half of the maximum amplitude. Sixteen images of the beam profile for each distance from the lens were averaged, and the FWHM was calculated in MATLAB.

Another key piece of information necessary for quantitative measurements was how much energy existed in each laser pulse. This was especially critical in the single-shot set of experiments because the laser energy fluctuated from shot to shot. Without knowledge of how much energy was incident upon the measurement volume, it would be impossible to correlate the observed scattering, fluorescence, or phosphorescence signals to a physical value. Calibration data of laser energy per pulse was collected in several different manners.

A beam splitter was placed in the optical train following the first turning mirror after the spectrometer separated the second and fourth harmonics of the Nd:YAG beam. This beam splitter was a circular glass plate that sampled approximately 10 percent of the 266nm beam, and directed it toward a photodiode (company/model #). An oscilloscope was used to observe the peak value and integrated signal measured by the photodiode.

Subsequently in the optical train, a flip mirror was positioned to redirect the laser beam onto a power meter. This tactic was used as another method of measuring the laser power. The power meter used offered several options, but the settings used in this study were to display the laser power, averaged over a 10-second period, in units of mW.

In situ measurements of laser energy were also recorded by both of the PI cameras. This was achieved by measuring the signal from a glass capillary tube in the vicinity of the measurement volume. The capillary was fastened to the droplet generator, and positioned it so that its tip was aligned with the laser sheet. Care was taken so that the capillary did not interfere with the laser light incident upon the measurement volume.

Each of the methodologies mentioned above were used to document measurements of laser power daily. The laser system and harmonic crystals were allowed to warm up for the appropriate amount of time of at least one hour before collecting the laser power calibration data. Then, measurements of laser power were recorded for polarizing wave plate positions of 0–90 degrees in 15-degree increments. The wave plate position that was chosen for the single-shot experiments described in Section 3.1.2 was 60 degrees because it bore the least amount of signal, and saturating the detector was a concern.

Section 3.1.4: Camera response

Prior to any fluorescence measurements being taken, a series of studies was conducted using a diffuse, broadband white light source. The purpose of these white light experiments was to gain a greater understanding of the camera response to adjustments in data collection settings such as exposure, gain, and the number of accumulations. A thorough knowledge of the collection device allows for appropriate corrections during data processing and the deduction of accurate conclusions. This series of white light studies was conducted on both the PI-MAX 4 camera used for laser-induced fluorescence measurements as well as the PI-MAX 4 camera used for Mie scattering measurements. The configuration used for this series of studies is shown in Figure 3.5.

PI-Max 4   ND Filter (used in pixel intensity study only)   Diffuser   White light source
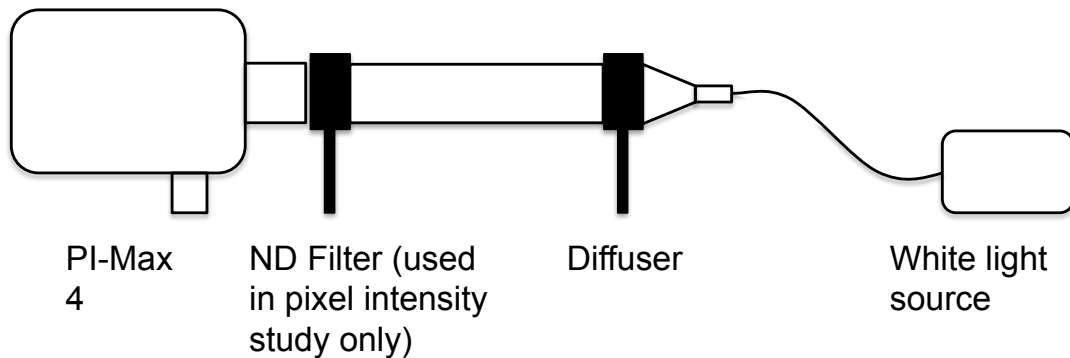
Figure 3.5: White light experimental setup.

A 150W flexible "snake light" constant power source was aligned to the collection device. The work described in this study utilized a Princeton Instruments PI-MAX 4 Intensified Charge-Coupled Device (ICCD) camera. For all experiments in this section, the camera was triggered internally. Prior to the light entering the camera lens, it passed through a ground glass diffuser in order to produce a more homogeneous intensity profile

and soften the effect of shadows from the source. During the pixel intensity study, various neutral density (ND) filters were positioned directly in front of the camera.

Section 3.1.4.1: Readout Noise Correction

For nearly all intensified charge-coupled devices, there exists an underlying level of background signal that presents itself in the results of scientific measurements. If unaccounted for, this background signal may unintentionally bias the result and lead to inaccurate conclusions. However, proper corrections are possible in the form of background subtraction. The focus of this experiment was to measure the value of the background signal for each camera.

The setup for this study was extremely simple, as there was no light source used and the lens was capped. Data was collected on both cameras for a range of the number of accumulations, as well as at multiple gain settings and exposure durations. Each background investigation file consisted of 100 frames that were averaged to determine a representative value of the background signal for each pixel. At the beginning of data processing, a background image with camera settings that matched the settings during respective data collection was subtracted from the droplet image to correct for the underlying background signal.

Section 3.1.4.2: Pixel Intensity Study

The goal of the pixel intensity study was to discern the range where the value measured by the camera pixels represent the true value of light entering the lens. The main principle behind this study is the Beer-Lambert Law, which states that the light

transmitted by a material, Φ_e^t, is related to the light received by the sample, Φ_e^i, and the absorbance of that material, A. The Beer-Lambert Law is expressed mathematically as

$$\frac{\Phi_e^t}{\Phi_e^i} = 10^{-A}.$$

The absorbance of a material can be described as the product of the molar attenuation coefficient, ε, the molar concentration of the material, c, and the path length, l, of the light as it attenuates through the sample. This relation is described symbolically as

$$A = \varepsilon * c * l$$

A PI-MAX 4 camera collected images of the white light source with various neutral density (ND) filters serving as mechanisms of light attenuation. The filters used during this study were 50mm diameter Edmund Optics UV-VIS ND filters with optical densities of 0.3, 0.5, 1.0, and 2.0. The filters were also stacked to simulate the effects of 1.3, 1.5, and 3.0 OD filters. Increasing the number of data points yielded a more comprehensive study on the performance of the ND filters. Images were also collected with no filter present to serve as a baseline. All camera settings such as trigger delay, exposure, intensifier gain, and the number of accumulations remained constant while collecting data for this study. The results of this study are shown below in Figure 3.6.
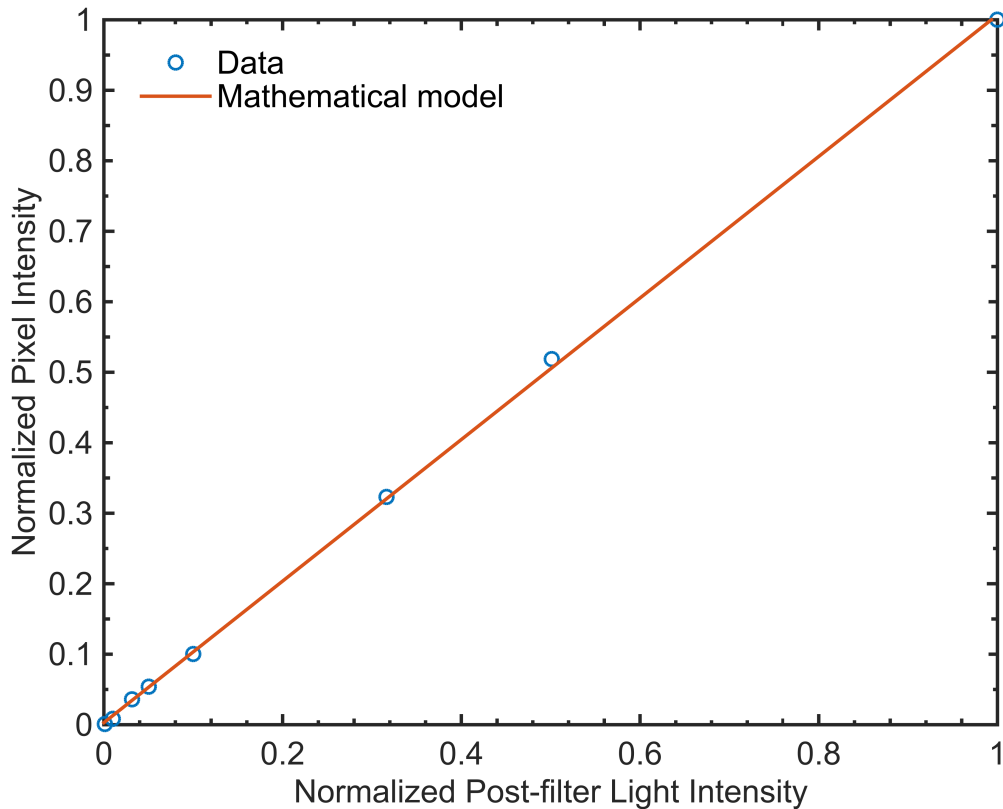
Figure 3.6: PI-MAX 4 pixel intensity study with white light source.

The linear behavior shown in this figure demonstrates the ability of the camera to accurately measure the intensity of the light source. For example, take the case of the ND filter with an optical density of 0.3. According to the Beer-Lambert Law, this filter should theoretically reduce the intensity of light observed by the collection device by 50 percent. The value of light intensity collected by the camera after passing through this filter is approximately 52 percent of the intensity collected when no filter was present. Data shown in Figure 3.6 coincide with the mathematical prediction for all filters used in the pixel intensity study. Hence, the intensity measured by the detector represents the true value of incident light for the range of the camera.

Section 3.1.4.3: Accumulation Study

The number of images that are collected onto the chip for a specific frame is defined as the number of accumulations. An increase in the on-chip accumulations leads to an increase in the value of the measured signal observed by the camera, which can be an extremely valuable tool when attempting to measure low-intensity signals. Consider this manipulation of camera settings to be a "stacking" of the images where regions of high intensity are compounded, leading toward a greater contrast with areas of lesser signal. The areas of lesser signal are also compounded, but because the intensity of the light is less in these regions, increasing the number of accumulations has less of an effect. Even when enhancing the contrast, a correction must be made when analyzing data that accounts for the accumulation setting in order to represent the true behavior of the object under examination.
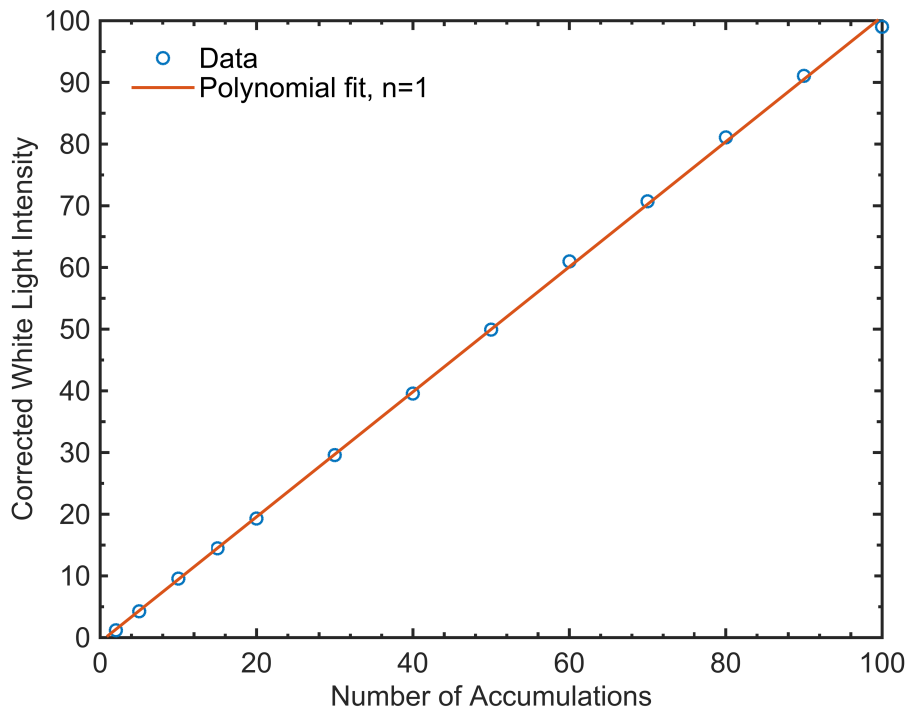

Figure 3.7: PI-MAX 4 accumulation study with white light source.

The primary goal of the accumulation study was to develop a correction method to be used in data processing that accounts for changes in the number of accumulations from dataset to dataset without requiring extensive adjustments in the processing code after each change in accumulation. Similar requirements exist for other camera parameters such as exposure and intensifier gain. The simplest way to correct for adjustments in camera parameters is to determine the range where each parameter behaves linearly. Once this range has been found, experiments can be tailored specifically so that the camera settings remain in the linear regime during data collection. For this study, the experimental setup described at the beginning of this section in Figure 3.5 was used to collect white light images. The exposure duration was set to 100 ns, and the intensifier gain was set to a value of 1 for the entire range of accumulation settings, and the trigger delay was held constant. The behavior of the data shown in Figure 3.7 indicates that the accumulation setting can be accounted for with a simple linear correction.

Section 3.1.4.4: Exposure Study

Another parameter that affects the amount of light captured by the camera is its exposure. More light, and therefore more signal, is collected as the exposure (also known as gate width) is increased. Because of the short lifetime of laser-induced fluorescence, it is advantageous to use a very short exposure. A short exposure is also useful when observing dynamic environments, as a large gate width can lead to blurring of a moving sample.

The goal of the exposure study was to determine the region where the exposure behaved linearly, similar to the accumulation response. A secondary goal was to measure the rise time of the camera exposure. This allowed the determination of the shortest usable

exposure after the camera response had reached a steady state. The setup illustrated in

Figure 3.5 was used in this experiment as well. During data collection, the trigger delay,

intensifier gain, and number of accumulations remained constant throughout the

experiment, while the gate width varied from 10–200ns.

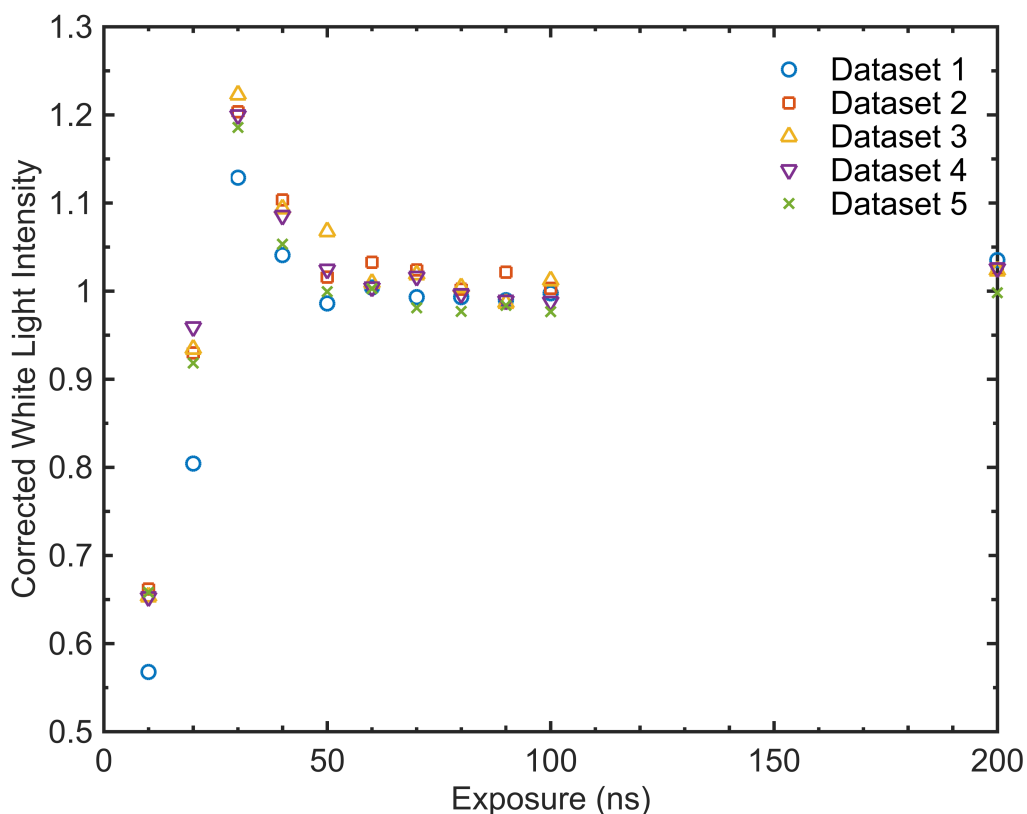**Figure 3.8: PI-MAX 4 exposure study with white light source.**

The results of the exposure study are shown in Figure 3.8. It was observed that the

rise and settling time of the camera is approximately 50ns, which helped govern the gate

width and delay settings for fluorescence lifetime measurements. A total of five data sets

were taken in an attempt to minimize noise affecting the conclusion of the experiment.

Section 3.1.4.5: Gain Study

Similar to how the number of accumulations may be adjusted to stack the signal observed by the camera, the intensifier gain setting may be adjusted to amplify the signal observed by the camera. However, rather than compound the images collected on the chip, the intensifier acts as a multiplier for the signal observed in every pixel of the frame. Therefore, the gain setting should affect the entire image equally, unlike the accumulation setting. As for all camera settings, the intensifier gain must be accounted for during data processing.

A study was conducted to establish the range of linear behavior for the intensifier gain. As with the other studies in this section, the setup shown in Figure 3.5 was used for this experiment. For a set number of accumulations, white light images were collected with the gain varying from 2–36 percent of the maximum intensifier gain. After the sweep of gain settings was completed, a new set of images was collected for a different number of accumulations. The numbers of accumulations used for this study were 2, 5, 10, 20, and 50. The trigger delay and exposure remained constant throughout the duration of this study. Results are shown in Figure 3.9, and a corrected plot where the measured values were divided by the respective gain setting is shown in Figure 3.10.
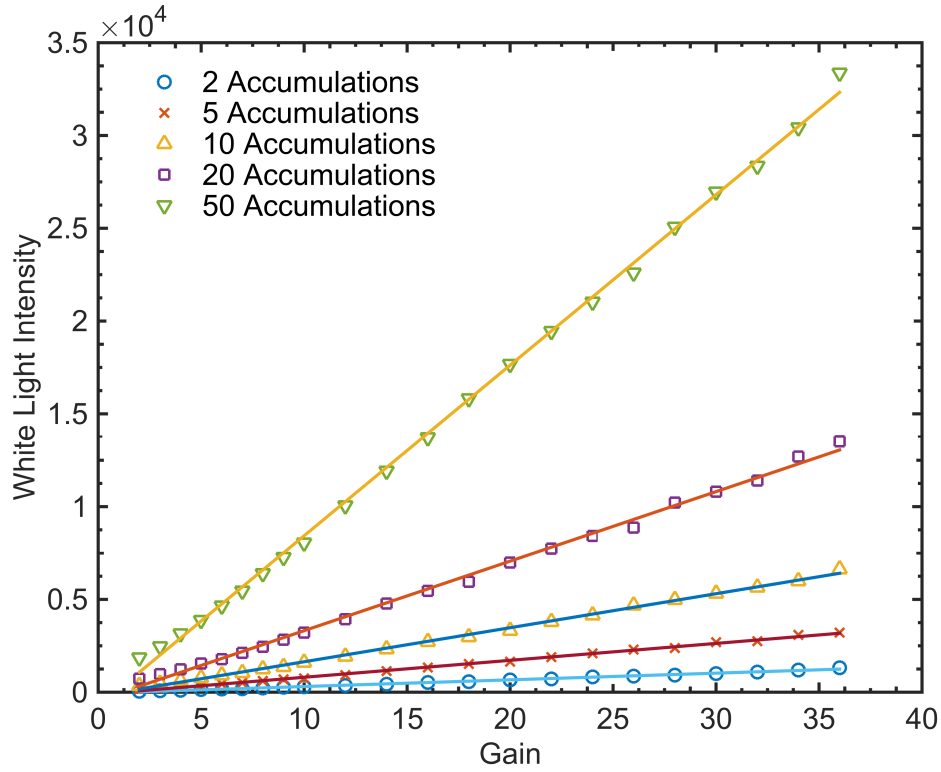
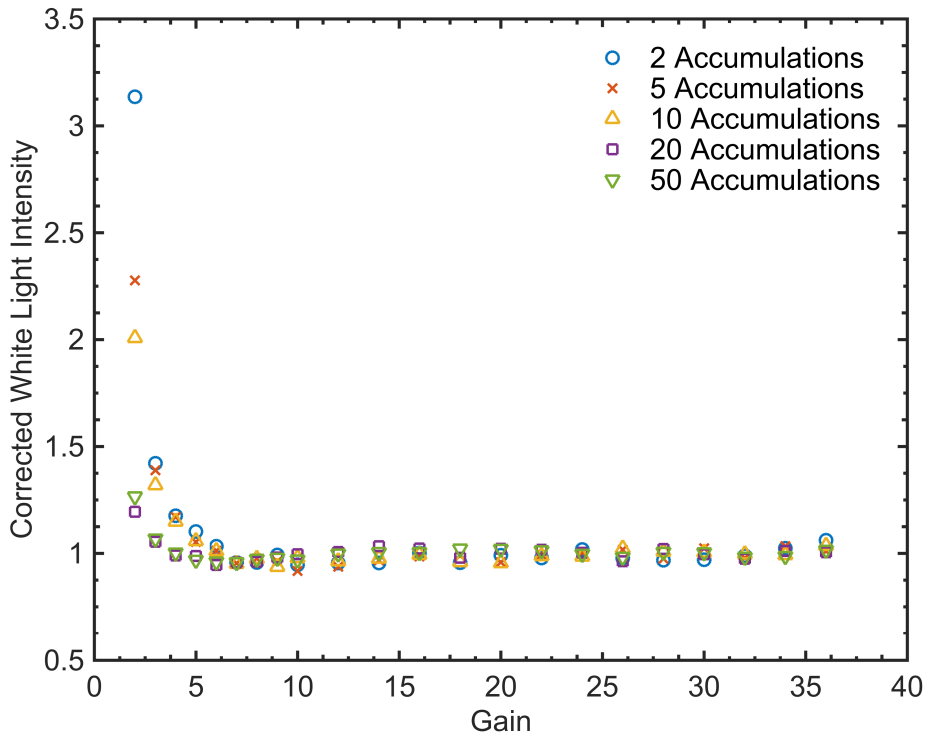**Figure 3.9: PI-MAX 4 intensifier gain study with white light source.**

Figure 3.10: Corrected PI-MAX 4 intensifier gain study with white light source.

It is quite clear from Figure 3.10 that the initial camera response to adjusting the intensifier gain is extremely non-linear. Therefore, it was determined that only gain settings at 10 percent or above—where the camera response has reached a steady, linear behavior—will be used in all further experiments.

Section 3.1.5: Test apparatus

A droplet generator (MicroFab MJ-SF-04) was positioned so that it would eject a monodisperse stream of droplets horizontally across the field of view of the cameras. The reservoir of the droplet generator was pressurized with nitrogen gas to force the droplets through an orifice in a miniscule glass tip. Two different tips were used with orifice sizes of 40μm and 80μm. A piezoelectric oscillator within the droplet generator controlled droplet size, spacing, and stability. An arbitrary function generator (Tektronix AFG 2021) was used to create a pulse that would initially be sent to a high voltage, inverting amplifier (Thorlabs HVA200) with –20 times amplification, and then relayed to the piezoelectric oscillator in the droplet generator. The baseline pulse parameters during standard operation were as follows: pulse width of 42μs not including a rise and fall time of 5μs, operating frequency of 2.0 kHz, high-level amplitude of 0 V, and low-level amplitude of -1.0 V. Generally, the supply pressure was approximately 30 mbar, however the droplet behavior was such that stability was difficult to maintain so the supply pressure and pulse parameters were subject to minor variation on a day-to-day basis.

The monodisperse droplet stream was injected into a perpendicular cross flow. Each experiment used two separate cross flow gases: pure nitrogen, and air (~20% oxygen

and 80% nitrogen). Regardless of the cross flow composition, the gas was conditioned

using the same method for each test. An in-line preheater and flexible heaters wrapped

around the stainless steel cross flow nozzle were used to elevate the gas temperature to

approximately 315°C. The temperature was measured with a Type K thermocouple

(OMEGA Engineering) at the outlet of the cross flow nozzle, below the measurement

volume. In order to increase the likelihood of consistently stable droplets, a bed of glass

spheres and a honeycomb were placed inside the cross flow nozzle to ensure uniform

laminar flow at its outlet. Mass flow controllers were used to maintain the cross flow

velocity at 1m/s at the outlet of the nozzle. After passing through the cross flow, the

droplet stream was drained into an electrically grounded, stainless steel vessel. This

allowed the spent fuel to be disposed of easily and appropriately.

An important behavior to characterize in order to understand the interaction

between the laser pulse and the droplets was the bulk motion of the droplet stream.

Accurate fluorescence, phosphorescence, or Mie scattering measurements would not have

been possible if the droplets demonstrated movement in and out of the laser sheet,

especially since the nature of this behavior would likely be intermittent. The transverse

motion of the droplet stream was measured to determine how much the droplets moved in

and out of the plane of the laser sheet. In order to accomplish this task, a mirror was placed

at an angle directly above the stream to relay the image onto the Point Grey camera. The

results showed that the droplet stream only exhibited minor motion in the transverse

direction. The range of motion was less than 4 pixels, which corresponds to approximately

14.8μm, or only approximately 6% of a typical droplet diameter. Thus, droplet movement

in and out of the plane of the laser was not a concern when the droplets were correctly

centered within the sheet.

Fuel was prepared for experimentation using the sparging technique mentioned at

the end of Chapter 2. Sparging was used as a method of saturating the liquid fuel with a

selected gas. As a result, the fuel was purged of gasses different that the gas used for

sparging. This process exploits the quenching effect that has been observed in the

presence of certain molecules, such as oxygen. By sparging liquid fuel with oxygen,

dissolved nitrogen is displaced and removed from the fuel. Theoretically, this should cause

a drop in the observed fluorescence and phosphorescence signals. The opposite is

proposed for nitrogen sparging.

The sparging system was designed from Swagelok components, and consisted of a

500 mL stainless steel cylindrical container with a dipstick placed along its center axis. At

the end of the dipstick was a carbonation stone to increase the surface area of the

interaction between the sparge gas and the liquid. A diagram of the sparging system can be

seen in Figure 3.11. A quarter-turn valve sealed the container at the bottom during

sparging, and allowed for simple and effective transfer of fuel. A long exhaust pipe that

extended to the height of the room's ceiling hood prevented pressure build-up, and safely

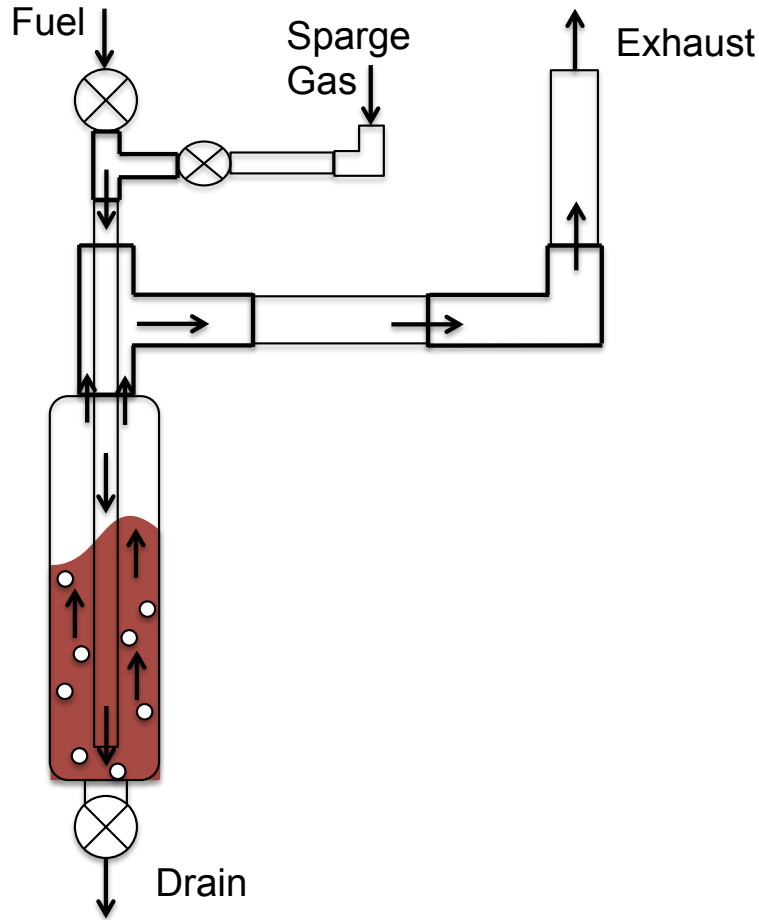directed any fumes and gases out of the facility.

Figure 3.11: Schematic of sparging cylinder.

A series of quarter-turn valves functioned as a manifold to provide control for which gas lines were open during sparging. Nitrogen, air, and pure oxygen were used as sparging gasses. Mass flow controllers were used to enable blends of different concentrations of oxygen and nitrogen

The concept of saturating jet fuel with pure oxygen gas raised serious safety concerns, and a system was designed accordingly to prevent and prepare for catastrophic events. First of all, the sparging container itself was chosen to be stainless steel, and was open to atmospheric pressure at all times. Guaranteeing that the liquid would not be pressurized alleviated concerns of unexpected detonation. Secondly, the source of oxygen

gas was a wall-mounted pressurized cylinder located in the back corner of the room, away from the sparging cylinder and the heated cross flow. A pneumatic valve controlled the flow of oxygen. In the default position, two springs forced the valve closed. When a supply of nitrogen gas was applied to the pneumatic valve, two pistons forced the valve open, allowing oxygen gas to flow to the sparging cylinder. An emergency shut-off valve controlled the supply of nitrogen to the pneumatic valve. This emergency shut-off valve was fastened to the corner of the experimental table, near the operating location of experimentalists during data collection. In the event of a fire, this emergency valve would have been closed, and all personnel would have had a clear escape route to the door of the lab.

CHAPTER 4

RESULTS AND DISCUSSION

The following chapter showcases selections of the data collected and discusses the results. Initial results of sparging experiments that were completed with acetone were used to characterize the system, and investigate the effects of sparging on a fuel tracer whose photophysical properties are well known. Results of experiments that were completed with Jet-A are presented in Section 4.2. This section discusses results of both time-averaged and single-shot testing.

Section 4.1: Characterization

The goal of the first set of experiments was to determine the effects of sparging on a monodisperse, liquid droplet stream. Characterization of the system was completed using acetone as a fuel surrogate during the initial investigation. Acetone was sparged for 30 minutes at a gas flow rate of 10.0 liters per minute. Measurements were taken for nitrogen-sparged and air-sparged fuel. A dataset of non-sparged acetone measurements was also taken as a baseline for comparison. For all three sparging cases, the cross flow was a 50-50 blend of pure nitrogen and air, resulting in a final composition of approximately 10 percent oxygen and 90 percent nitrogen. The cross flow was room temperature (approximately 20°C) throughout the duration of the acetone experiments. Time-averaged data points of 50 accumulations each were collected to measure the acetone phosphorescence lifetime. Timing for the PI camera that was measuring LIF/LIP is

detailed in the following paragraph. The settings of the PI camera measuring Mie

scattering were held constant for all data points of the decay curve.

In order to prevent the measurement of scattered laser light, and to avoid jitter in

the laser pulse, the exposure for the first data point began approximately 10 ns after the

laser pulse was incident on the droplets. Based on the behavior observed in the camera

response studies, the gate width for the first data point was 50 ns. This same exposure

setting was used up to approximately 110 ns after the pulse. After this delay setting, the

exposure was adjusted to increase the signal observed by the camera. Data points were

collected in steps of 50 ns until the measured signal was close to the background noise

level of the camera. The intensifier gain settings were adjusted as needed, and care was

taken to remain in the linear region of the gain curve as described in the camera response

studies. Further details of the LIF/LIP PI camera settings are available in Table 4.1.

Table 4.1: LIF/LIP PI-MAX 4 camera settings for acetone lifetime measurements.

Delay relative to laser pulse (ns)	Exposure (ns)	Intensifier gain (%)	Number of accumulations
10	50	1	50
60	50	10	50
110	50	10	50
160	100	14	50
260	200	14	50

A sample image of the droplets from the time-averaged experiments is shown in Figure 4.1,
and the data collected in the experiment described above is shown below in Figure 4.2.
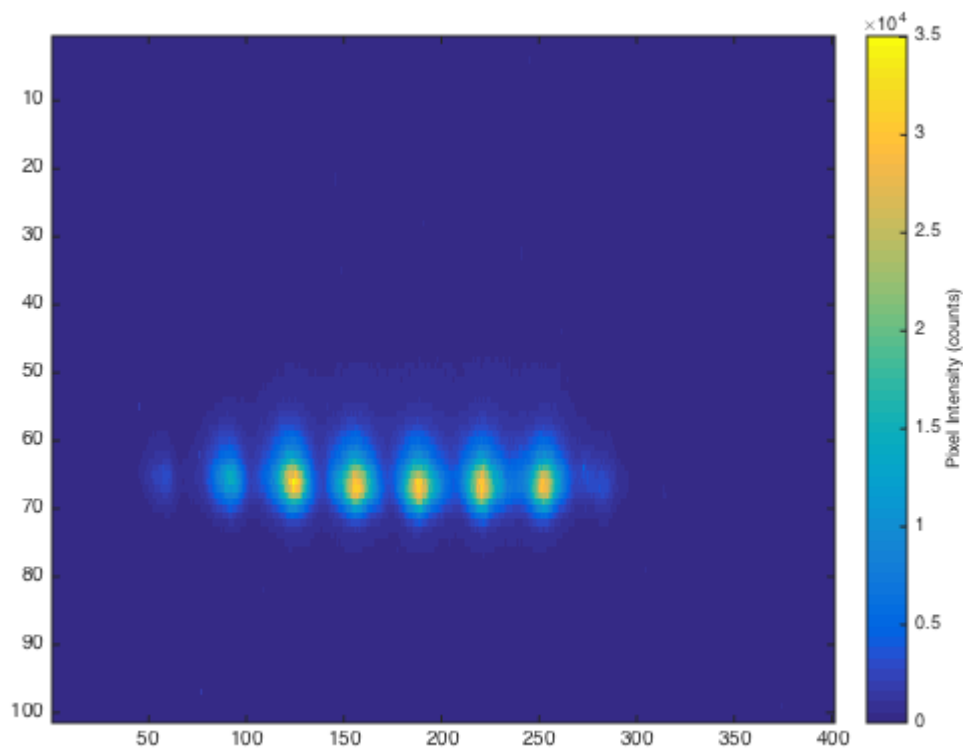
Figure 4.1: Monodisperse stream of nitrogen-sparged acetone droplets in a nitrogen cross flow.
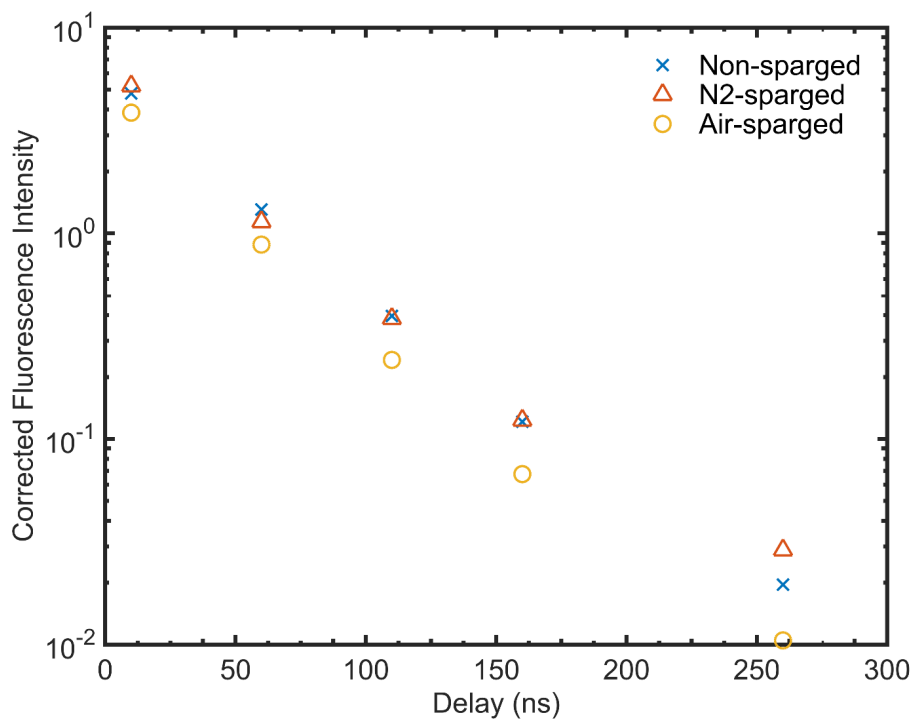

Figure 4.2: Acetone lifetime data with blended cross flow.

Notice that there is not a significant difference among the three sparging cases. This data shows that the presence of oxygen in the cross flow, and the ensuing effect of quenching, significantly affected the results. In a pure nitrogen cross flow, sparging would be expected to have a much larger impact. From this point onward, all experiments would be repeated for two cross flow conditions: pure nitrogen and air (approximately 20 percent oxygen and 80 percent nitrogen). Data for the acetone experiments under these improved cross flow conditions are presented below in Figures 4.3 and 4.4. The former shows the lifetime decay on a logarithmic y-axis, while the latter illustrates the rate of decay as normalized to the initial data point for each sparging and cross flow combination. An important distinction between these two figures is the difference between the terms "corrected" and "normalized". Corrected values are those that have been appropriately adjusted for changes in camera parameters, as discussed in Section 3.1.4. The term "normalized" designates that the data has been divided by the first data point for each series.
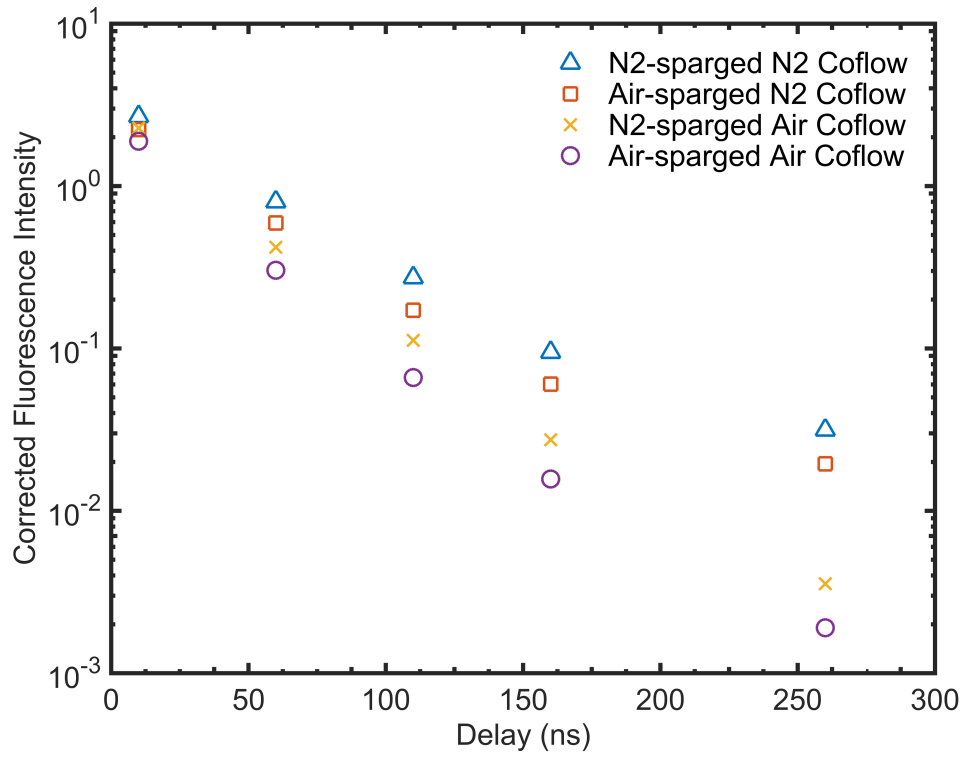
Figure 4.3: Effects of cross flow gas composition on acetone LIF/LIP signals.
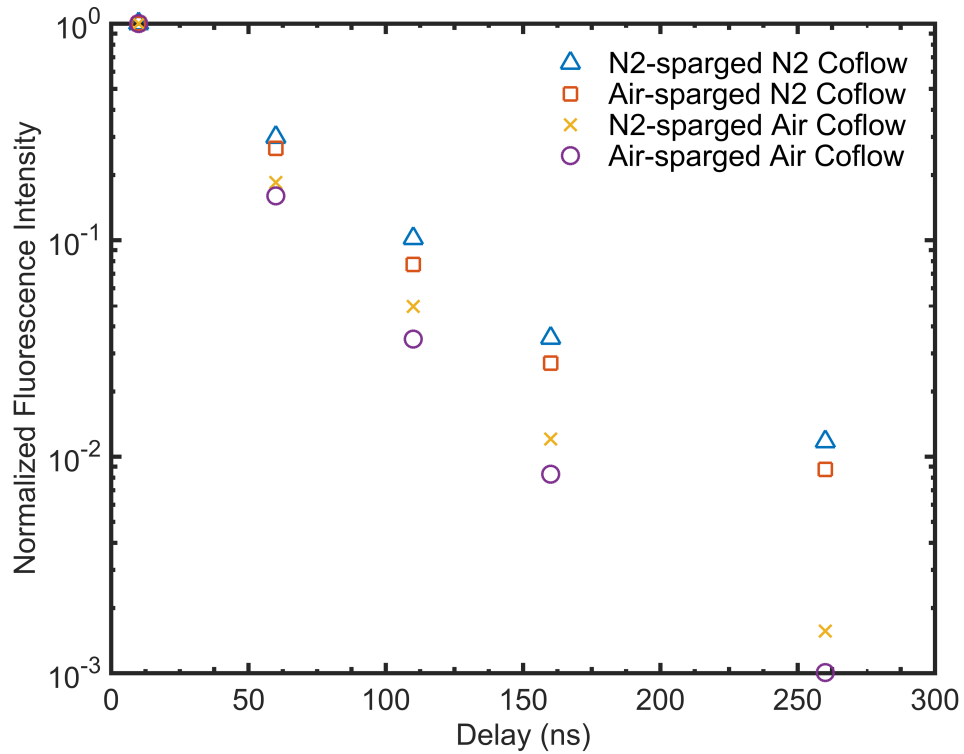

Figure 4.4: Effects of cross flow gas composition on acetone LIF/LIP rate of decay.

The general effect of the presence of oxygen in the cross flow as well as in the sparge gas is noticeable, as these cases show lower signal intensity and have a faster rate of decay. However, the presence of oxygen in the cross flow dominates the effects of sparging.

Section 4.2: Jet-A Experiments

An important concept to the study of spray measurements is the differences between different classes of fluorescing molecules. The different responses between ketones (such as acetone) and aromatics (like those found in fuels) to sparging require further investigation for complete understanding. In an attempt to answer this question, a similar set of experiments to the acetone study described above was completed with Jet-A. Jet-A is a mid-grade aviation fuel that can be considered to be representative of a general fuel used in aerospace applications. Other than the fuel used, there are a few key differences to this set of experiments compared to the acetone experiments. First of all, in the Jet-A study the cross flow was heated to approximately 320°C. This temperature was selected because it is approximately 100°C higher than the top of the distillation curve of Jet-A. An extreme difference between the temperature of the environment and the boiling point of Jet-A is necessary to vaporize the fuel on the short time-scale as it passes through the cross flow. Another notable difference between the Jet-A and acetone studies is the addition of different sparge gas compositions. Blends of oxygen and nitrogen with increasing oxygen concentration—to the point of 100 percent oxygen—were used in the Jet-A experiments. A complete list of the combinations of sparge and cross flow compositions is available in Table 4.2.

Table 4.2: Sparge gas and cross flow composition conditions.

Sparge gas composition	Cross flow composition
100% Nitrogen	100% Nitrogen
20% Oxygen, 80% Nitrogen (air)	100% Nitrogen
40% Oxygen, 60% Nitrogen	100% Nitrogen
60% Oxygen, 40% Nitrogen	100% Nitrogen
80% Oxygen, 20% Nitrogen	100% Nitrogen
100% Oxygen	100% Nitrogen
100% Nitrogen	20% Oxygen, 80% Nitrogen (air)
20% Oxygen, 80% Nitrogen (air)	20% Oxygen, 80% Nitrogen (air)
40% Oxygen, 60% Nitrogen	20% Oxygen, 80% Nitrogen (air)
60% Oxygen, 40% Nitrogen	20% Oxygen, 80% Nitrogen (air)
80% Oxygen, 20% Nitrogen	20% Oxygen, 80% Nitrogen (air)
100% Oxygen	20% Oxygen, 80% Nitrogen (air)

The remainder of this section presents two sets of experiments. The first study that will be discussed involved time-averaged measurements of laser-induced fluorescence of the monodisperse droplet stream. The second set of experiments that will be presented here is a study of the droplet stream where measurements of Mie scattering and LIF were taken on a shot-by-shot basis. Both sets of experiments utilized an extremely similar setup and testing procedure. The main difference between these two studies was that the time-averaged study captured several accumulations of images on each frame, whereas the single-shot study was limited to a single exposure for each frame of data.

Once the PI cameras were synced with the laser via the DAT method described in Section 3.1 the temporal value of the peak of the laser pulse was found with respect to each camera by setting the exposure to 10 ns and stepping through the gate delay until the maximum signal was found. It was important for the signal to be extinct once the laser pulse was over, so this timing study was completed by observing Mie scattering from isopropanol droplets. All other camera settings were maintained at a constant value as the

delay relative to the laser pulse swept through a range of values until the timing of the peak

signal was observed.

Section 4.2.1: Time-averaged experiments

As with the acetone experiments described above, fluorescence and

phosphorescence lifetime decay measurements of Jet-A were recorded. Because of

differences in the photophysical behavior between the two fuels, the fluorescence and

phosphorescence intensities varied. For this reason, there adjustments had to be made in

the camera settings for the Jet-A experiments to avoid saturating the detector. The camera

settings used in the Jet-A study are listed in Table 4.3.

Table 4.3: LIF/LIP PI-MAX 4 settings for Jet-A heated cross flow experiments.

Delay relative to laser pulse (ns)	Exposure (ns)	Intensifier gain (%)	Number of accumulations
15	50	1	50
40	50	1	50
65	50	1	50
165	200	1	50

The lifetime decay curves on a logarithmic y-axis for a variety of sparge gas compositions

are displayed below in pure nitrogen cross flow in Figure 4.5 and an air cross flow in Figure

4.6. The data in these two plots have been fitted with a two-term exponential decay
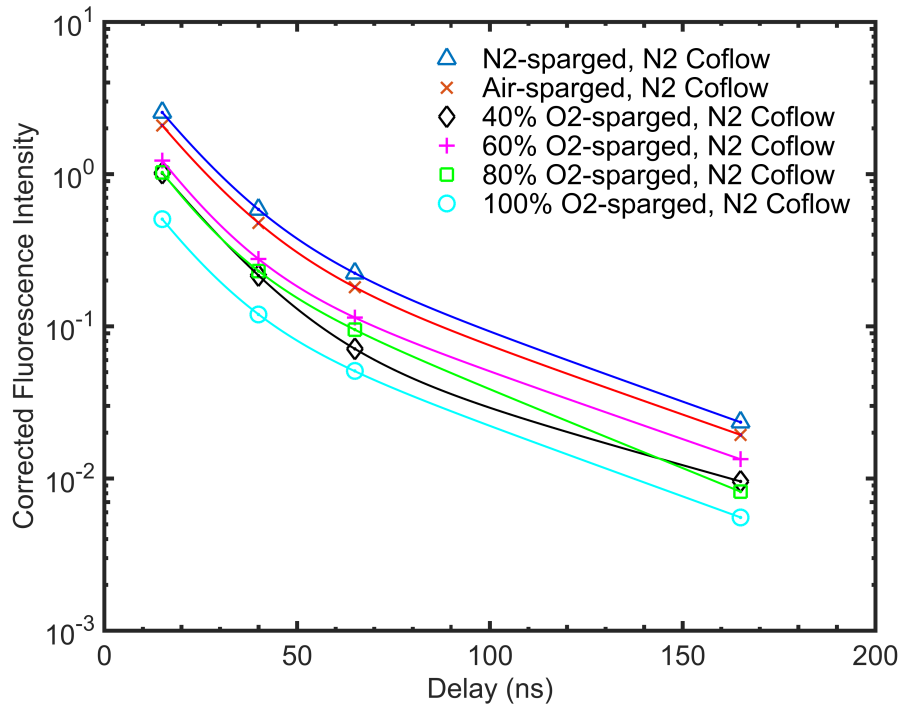
mathematical model.

Figure 4.5: Time-averaged LIF lifetime measurements for varying concentrations of oxygen in the sparge gas of Jet-A droplets in nitrogen cross flow.
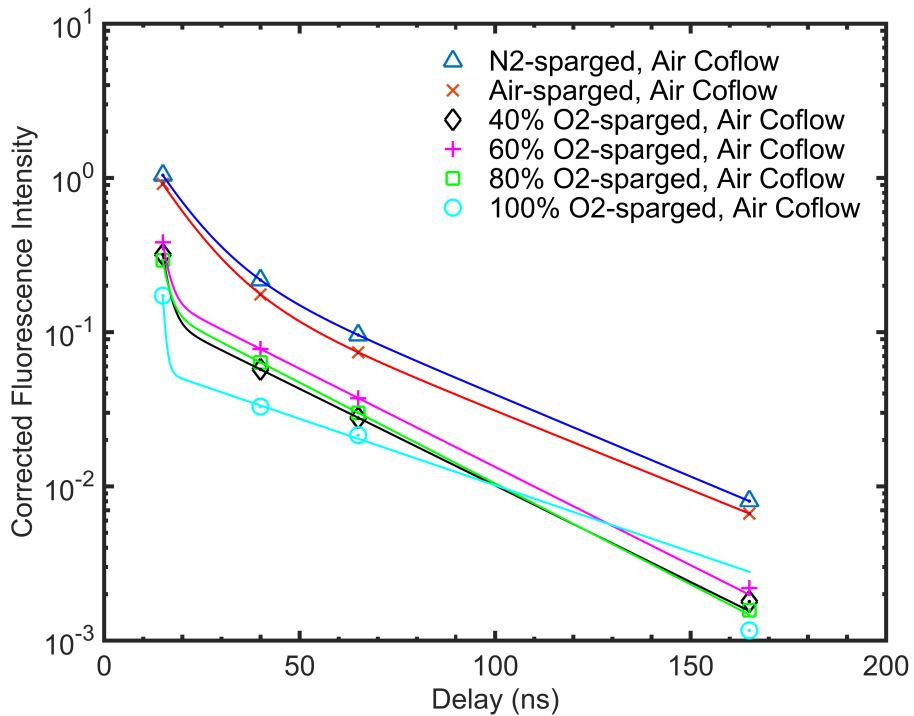

Figure 4.6: Time-averaged LIF lifetime measurements for varying concentrations of oxygen in the sparge gas of Jet-A droplets in air cross flow.

An interesting behavior is observed from these two figures. It appears as though for each cross flow the curves have the same shape regardless of the sparge gas composition, i.e. the data show a consistent rate of decay. The amount of oxygen present in the sparge gas appears to simply influence the initial intensity of the fluorescence signal. In other words, the sparge gas composition shifts the fluorescence intensity values up and down without affecting the decay rate. Increased levels of oxygen in the sparge gas show stronger signs of quenching, as would be expected. This conclusion is clearly evident when each sparge gas and cross flow condition is normalized by its first data point. The data points appear to overlap, supporting the observations described earlier in this paragraph. This is shown for nitrogen and air cross flows in Figure 4.7 and Figure 4.8, respectively. Unfortunately, the cause of this behavior is unknown, and requires further examination in order to be fully understood. However, it is certain that this behavior is very different than what was observed with acetone.

A second trend perceived from this data is that, once again, the presence of oxygen in the cross flow exhibited strong signs of quenching. This effect was so significant that it dominated the effects of sparging the fuel.
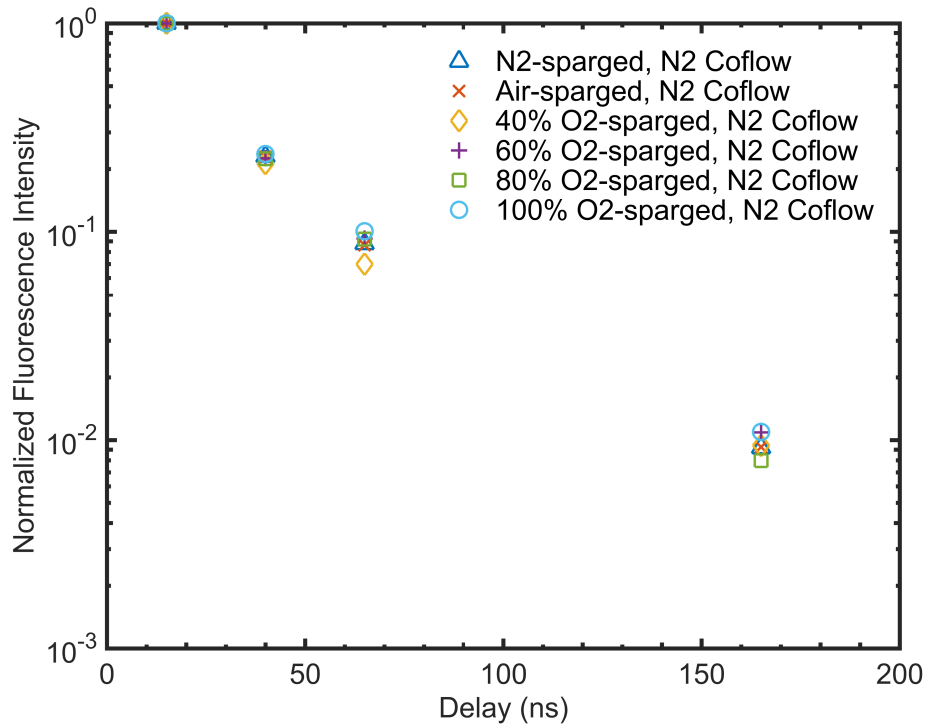
Figure 4.7: Normalized data of time-averaged LIF lifetime measurements for varying concentrations of oxygen in the sparge gas of Jet-A droplets in nitrogen cross flow.
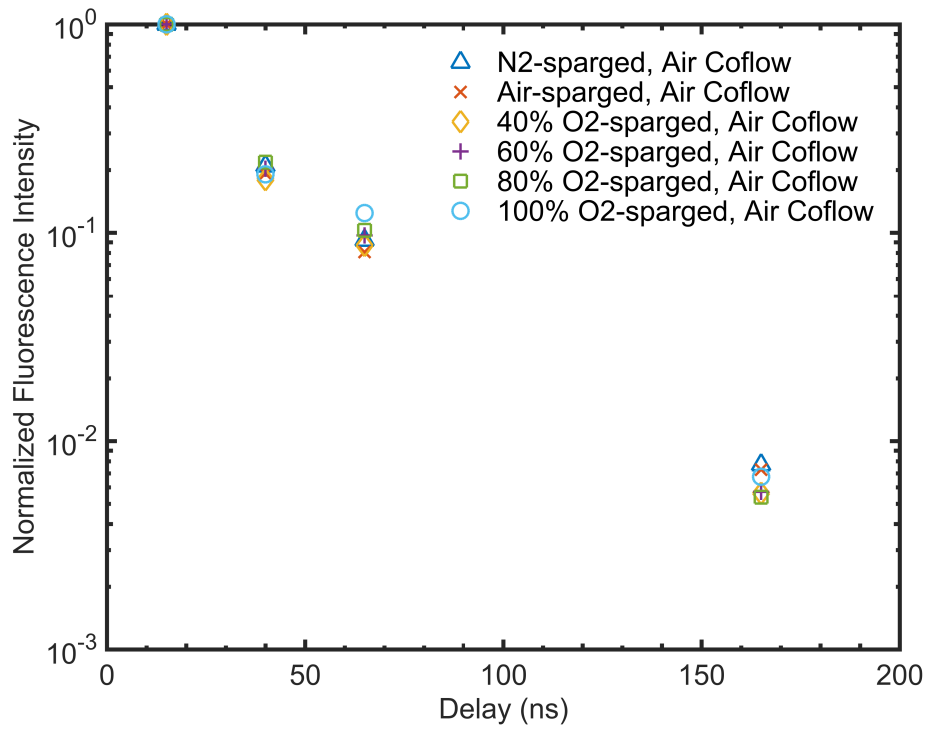

Figure 4.8: Normalized data of time-averaged LIF lifetime measurements for varying concentrations of oxygen in the sparge gas of Jet-A droplets in air cross flow.

Section 4.2.2: Single-shot experiments

Next, the same conditions were observed on a single-shot basis. Images were collected for a single instance of the interaction of the laser pulse with the droplet stream. This strategy hoped to provide a crisper image of the droplets. Figure 4.9 provides an example of a single-shot image, and it is clear that the shape of the droplets and vapor trails are much clearer and more visible compared to the time-averaged images. It should be noted that the dynamic range for these two images was modified to limit the upper value to 400 counts. This was necessary in order to for the vapor to be visible, as it was near the background noise level of the camera.

Measurements of the vapor signal were also considered during these experiments. The regions considered during data processing are shown in Figure 4.10. An area of pixels was selected around the droplets and the mean value was calculated to determine the signal from the liquid phase. Directly above the droplet stream, a larger area was selected and the mean intensity calculated to determine the value of the vapor signal. The structure in the northwest quadrant is a glass capillary used to calibrate for fluctuations in laser power on a shot-to-shot basis.

Table 4.4 shows the camera parameters used in the single-shot experiments. Negative delay values represent data taken before the arrival of the laser pulse. The delay step represents the change in the camera delay between incremented files.

Table 4.4: Single-shot experiment camera parameters.

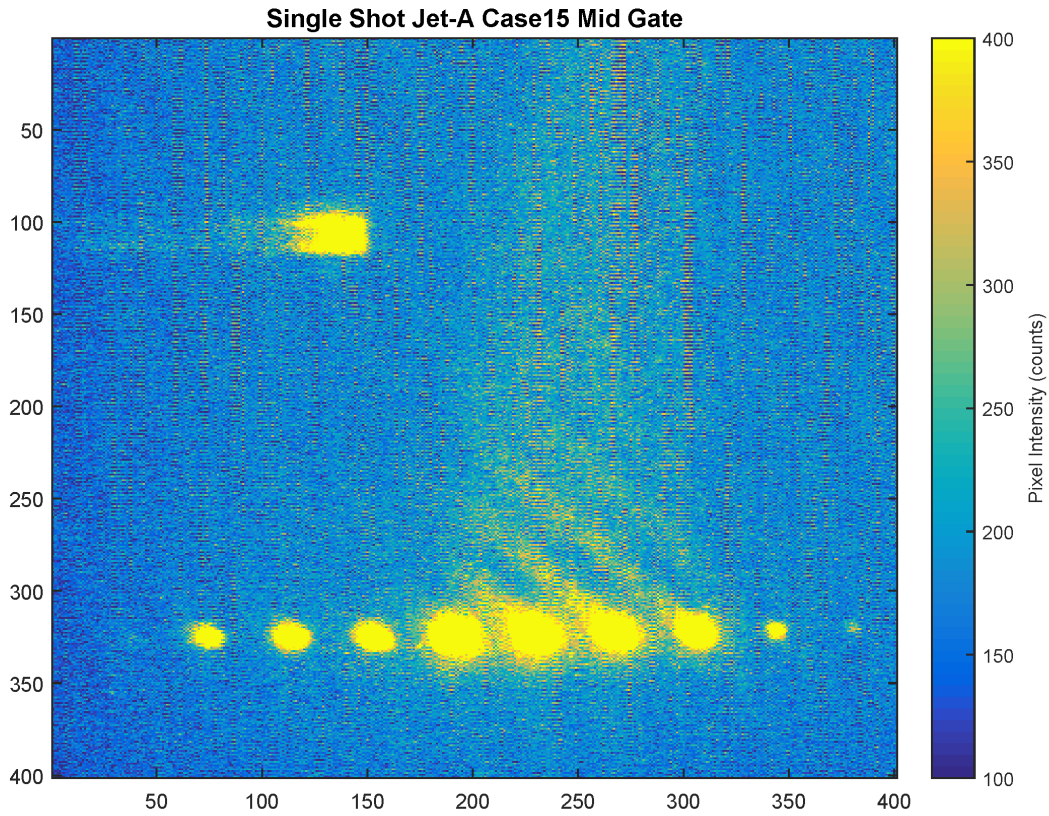| File increment	Delay relative to laser pulse (ns)	Delay step (ns)	Exposure (ns)	Intensifier gain (%)
1	-10	10	50	10
2–12	0–100	10	50	1
13–16	110–140	10	50	10
17–21	160–260	25	50	15
22–23	285–310	25	50	25
24–28	360–560	50	100	50
29–31	610–810	100	200	60

Figure 4.9: Single-shot image of 280µm diameter O2-sparged Jet-A droplets in a nitrogen cross flow. Captured at a delay of 110 ns relative to laser pulse.
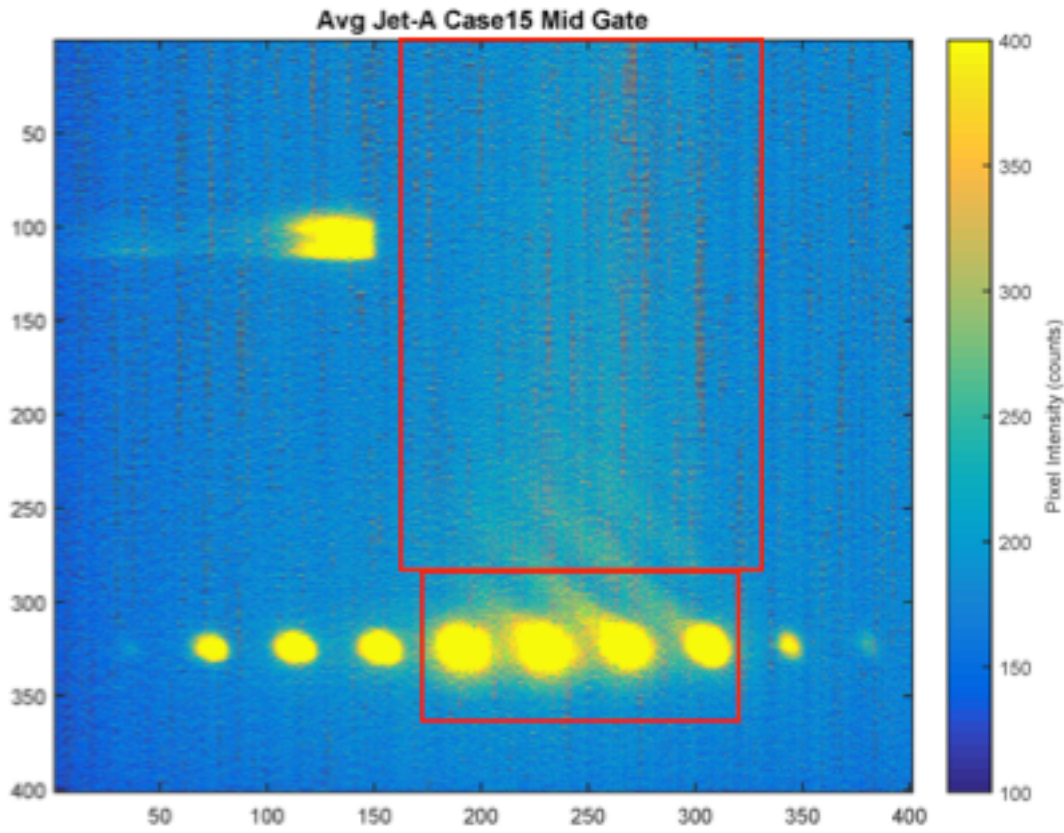
Figure 4.10: Average of 100 single-shot images of 280μm diameter O2-sparged Jet-A droplets in nitrogen cross flow. Captured at a delay of 110 ns relative to laser pulse.

Figure 4.11 and 4.12 provide examples of fluorescence lifetime single-shot measurements for Jet-A in the liquid-phase and vapor-phase, respectively. These data points represent the average value of 100 laser pulses, similar to the image in Figure 4.10. The case that was selected for Figure 4.11 and 4.12 was Jet-A that had been sparged with 80 percent oxygen and 20 percent nitrogen, and was entrained in a pure nitrogen cross flow. The error bars on the figures represent one standard deviation from the mean. It is evident that the data is fairly consistent among the 100 shots.
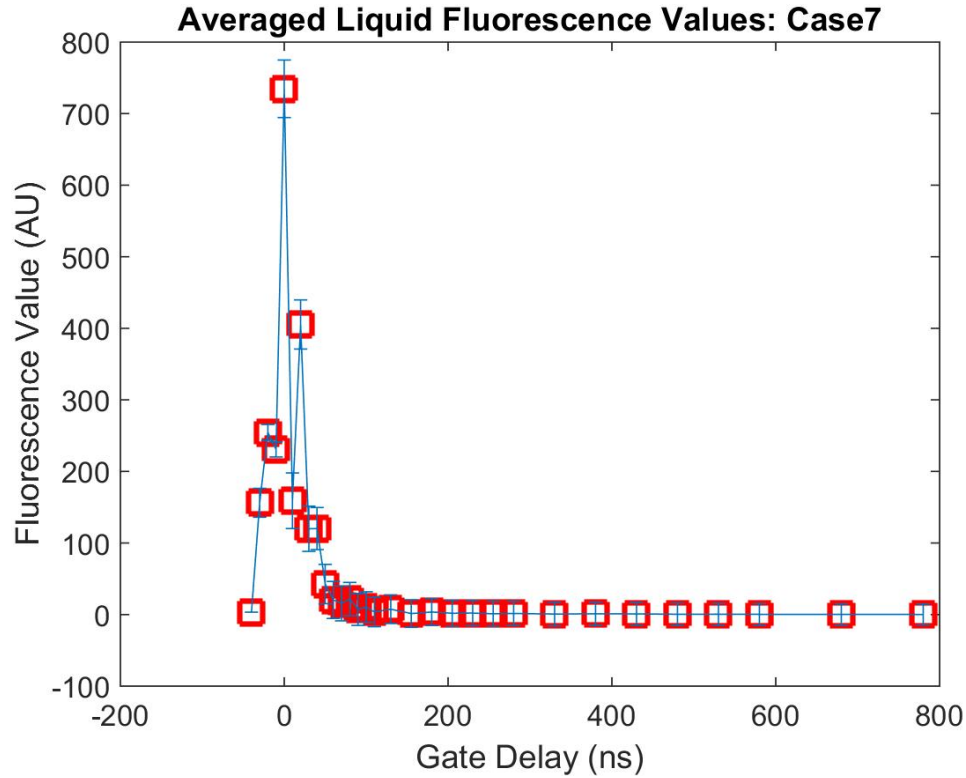
Figure 4.11: LIF decay curve for liquid Jet-A droplets sparged with 80% oxygen and 20% nitrogen in a nitrogen coflow. Error bars represent one standard deviation from the mean.
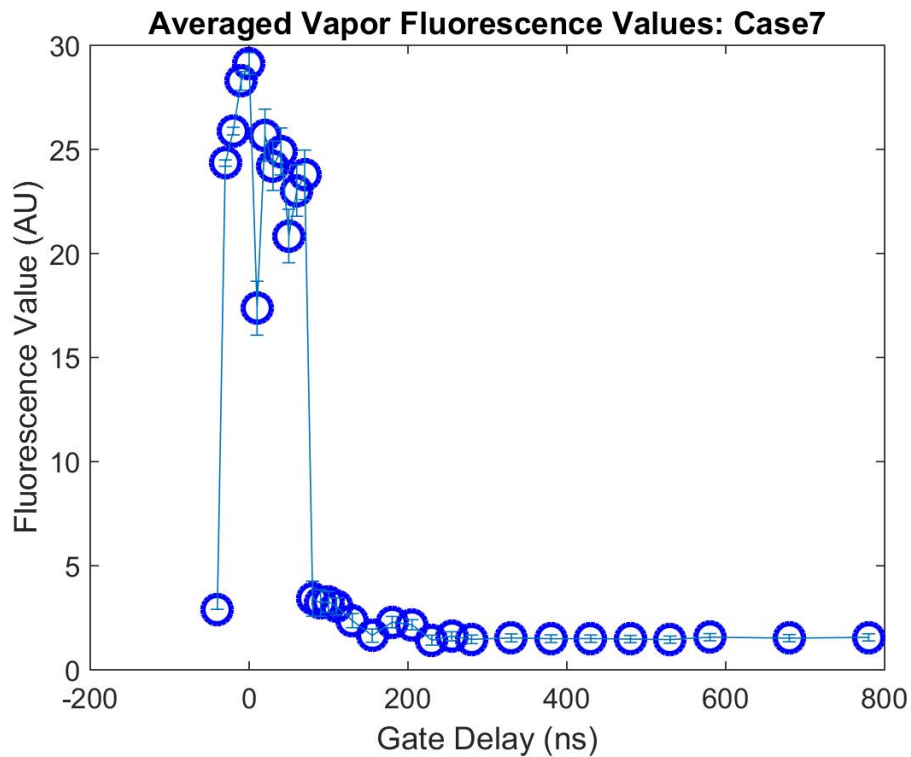

Figure 4.12: LIF decay curve for Jet-A vapor from fuel that was sparged with 80% oxygen and 20% nitrogen in a nitrogen coflow. Error bars represent one standard deviation from the mean.

The same data has been plotted with a logarithmic scale along the y-axis. It can be

seen that the liquid signal consistently decreases with time, whereas the vapor signal

shows a swift decay after the laser pulse, and then remains fairly constant. However, as

mentioned above, this consistent signal after showing initial values may be because the

vapor signal is so close to the background level and the values reported may be those of the
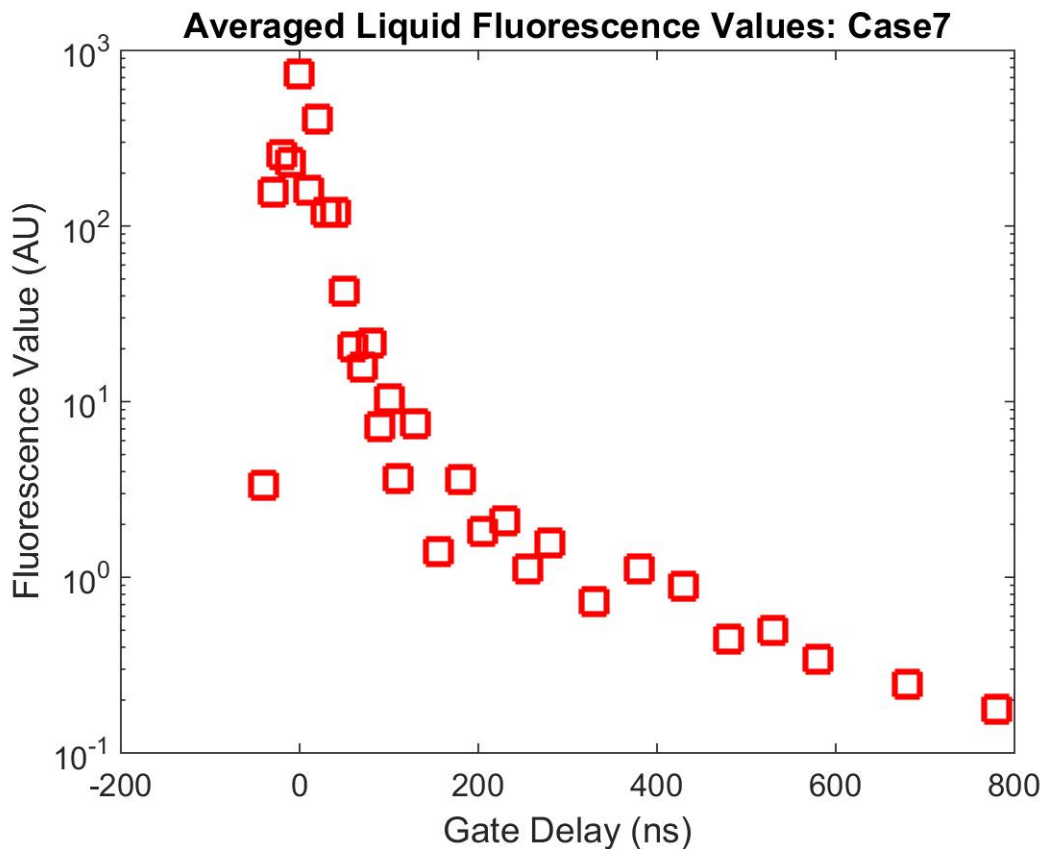
background noise.

Figure 4.13: Data shown in Figure 4.11 plotted on logarithmic scale for the y-axis.
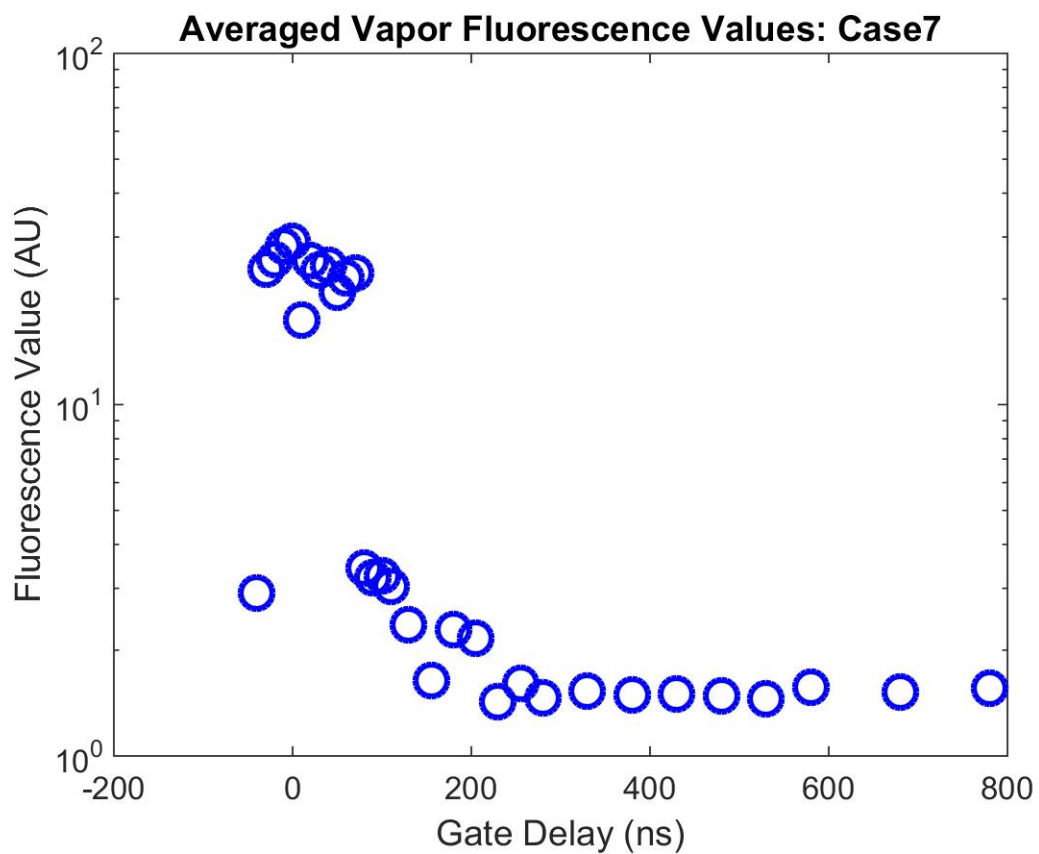
Figure 4.14: Data shown in Figure 4.12 plotted on logarithmic scale for the y-axis.

CHAPTER 5

CONCLUSIONS

In the final chapter of the current work, a summary of accomplished tasks is presented, challenges encountered are discussed, and recommendations for further investigation are made.

Section 5.1: Summary

The work described here attempted to accurately measure liquid- and vapor-phase mass distribution from a monodisperse droplet stream that was injected into a heated cross flow. Unfortunately, the strategies applied to this problem did not yield a successful result. A major goal of the experiments presented here was to determine the effect of sparging with oxygen in fuels, and compare the response to oxygen sparging in ketones. Significantly different behavior was observed between the quenching characteristics of aromatics and ketones. Ketones exhibited strong response to even trace quantities of oxygen. While aromatics did show some signs of collisional quenching from the presence of oxygen, the behavior was not as extreme as in acetone. This was especially true when comparing the effects of oxygen quenching when measuring the rate of decay. A possible explanation for this observation is the lack of phosphorescence emission in Jet-A, where ketones are readily populated in the triplet state.

A significant challenge throughout the entirety of the presented studies was the erratic behavior of the droplet generator. Inconsistent and unreliable performance caused variation in size and position of droplets. Although cumbersome, poor images could be

discarded when processing data from the single-shot measurements. However, avoidance of the unpredictable droplet behavior was impossible for the time-averaged experiments.

Section 5.2: Recommendations for Future Work

In order to advance the state of combustion systems and propulsion technology, thorough quantitative measurements must be completed in configurations that closely resemble an application. However, there is still much work that must be completed prior to achieving such a goal. Once a strategy for phase discrimination has been developed and demonstrates success with the monodisperse droplet stream, a suggested avenue to pursue is to introduce a known quantity of fuel vapor seeded into the cross flow. After a diagnostic approach provides positive results in that scenario, imaging a fine spray from a nebulizer, then a full spray through injection nozzles, should further test the technique until it is refined. Of course, variations in temperature and pressure must be investigated to gain a complete understanding of the behavior of multi-phase polydisperse sprays. It is quite possible that the strategies portrayed in this work are not capable of obtaining quantitative measurements on their own. Pairing these strategies with structured light techniques, for instance, may be effective for phase discrimination. Further investigation may also show that an entirely different method, such as X-ray radiography, would be a more prosperous avenue.

It is important that an additional consideration be made regarding alternate fuel compositions. Jet-A was a primary fuel used in the presented experiments, however its photophysical properties are different than two other common aviation fuels, JP-8 and JP-10. Promising fuel tracers also include naphthalene and toluene. Complete

characterization of each of these fuels and tracers is imperative for comprehensive

knowledge of the behavior of fuels in varying conditions. Furthermore, the only cross flow

environments that were considered throughout this study were pure nitrogen and air. A

greater range of oxygen in the cross flow should be implemented in order to extend the

study on the effects of oxygen quenching. Finally, some work has been completed

regarding the investigation of droplet size and laser sheet thickness. However, this work

was not comprehensive and further information may be available via these avenues.

BIBLIOGRAPHY

Allison, Patton M., Thomas A. McManus, and Jeffrey A. Sutton. 2016. "Quantitative Fuel Vapor/air Mixing Imaging in Droplet/gas Regions of an Evaporating Spray Flow Using Filtered Rayleigh Scattering." *Optics Letters* 41 (6): 1074. doi:10.1364/OL.41.001074.

"Annual Energy Review 2015," (U.S. Energy Information Administration, 2016).

Bachalo, W. D., and M. J. Houser. 1984. "Phase/Doppler Spray Analyzer for Simultaneous Measurements of Drop Size and Velocity Distributions." *Optical Engineering* 23 (5): 583–90.

Bachalo, William D. 1980. "Method for Measuring the Size and Velocity of Spheres by Dual-Beam Light-Scatter Interferometry." *Applied Optics* 19 (3): 363–70.

Berrocal, Edouard, Elias Kristensson, Mattias Richter, Mark Linne, and Marcus AldÚn. 2008. "Application of Structured Illumination for Multiple Scattering Suppression in Planar Laser Imaging of Dense Sprays." *Optics Express* 16 (22): 17870–81.

Bohren, C. F., and D. R. Huffman. 1983. *Absorption and Scattering of Light by Small Particles*. New York: John Wiley & Sons.

Charogiannis, Alexandros, and Frank Beyrau. 2013. "Laser Induced Phosphorescence Imaging for the Investigation of Evaporating Liquid Flows." *Experiments in Fluids* 54 (5). doi:10.1007/s00348-013-1518-2.

Chin, J. H., C. M. Sliepcevich, and M. Tribus. 1955a. "Determination of Particle Size Distributions in Polydispersed Systems by Means of Measurements of Angular Variation of Intensity of Forward-Scattered Light at Very Small Angles." *The Journal of Physical Chemistry* 59: 845–48.

Chin, J. H., C. M. Sliepcevich, and M. Tribus. 1955b. "Particle Size Distributions for Angular Variation of Intensity of Forward-Scattered Light at Very Small Angels." *The Journal of Physical Chemistry* 59: 841–44.

Copeland, Richard A., and David R. Crosley. 1985. "Radiative, Collisional and Dissociative Processes in Triplet Acetone." *Chemical Physics Letters* 115 (4): 362–68.

Dobbins, R. A., L. Crocco, and I. Glassman. 1963. "Measurement of Mean Particle Sizes of Sprays from Diffractively Scattered Light." *AIAA Journal* 1 (8): 1882–86. doi:10.2514/3.54946.

Dolovich, Myrna B., and Rajiv Dhand. 2011. "Aerosol Drug Delivery: Developments in Device Design and Clinical Use." *The Lancet* 377 (9770): 1032–45.

Eckbreth, A. C. 1996. *Laser Diagnostics for Combustion Temperature and Species*. 2nd Ed. Cambridge, Massachusetts: Abacus Press.

Farmer, W. Maxin. 1972. "Measurement of Particle Size, Number Density, and Velocity Using a Laser Interferometer." *Applied Optics* 11 (11): 2603–12.

Foreman, J. W., E. W. George, and R. D. Lewis. 1965. "Measurement of localized flow velocities in gases with a laser doppler flowmeter." *Applied Physics Letters* 7 (4): 77. doi:10.1063/1.1754319.

Forkey, J. N., N. D. Finkelstein, W. R. Lempert, and R. B. Miles. 1996. "Demonstration and Characterization of Filtered Rayleigh Scattering for Planar Velocity Measurements." *AIAA Journal* 34 (3): 442–48. doi:10.2514/3.13087.

Greenblatt, G. D., S. Ruhman, and Y. Haas. 1984. "Fluorescence Decay Kinetics of Acetone Vapour at Low Pressures." *Chemical Physics Letters* 112 (3).

Grossmann, F., P. B. Monkhouse, M. Ridder, V. Sick, and J. Wolfrum. 1996. "Temperature and Pressure Dependences of the Laser-Induced Fluorescence of Gas-Phase Acetone and 3-Pentanone." *Applied Physics B* 62 (3): 249–53.

Ingebo, R. D. 1957. "Atomization, Acceleration and Vaporization of Liquid Fuels." *Sixth Symposium (International) on Combustion*, 684–87.

John Deere. 2015. "Understanding Emissions Regulations." *Www.deere.com*. https://www.deere.com/en_US/services_and_support/engine-information/understanding-emission-regulations/understanding-emission-regulations.page.

Kiel, Barry V., James R. Gord, Jacob B. Schmidt, Joseph D. Miller, and Terrence R. Meyer. 2009. "Simultaneous Planar Fluorescence, Phosphorescence, and Mie Scattering in Pressure-Atomized Sprays." In *11th Triennial International Annual Conference on Liquid Atomization and Spray Systems, Vail (USA)*.

Kishawy, H.A., M. Dumitrescu, E.-G. Ng, and M.A. Elbestawi. 2005. "Effect of Coolant Strategy on Tool Performance, Chip Morphology and Surface Quality during High-Speed Machining of A356 Aluminum Alloy." *International Journal of Machine Tools and Manufacture* 45 (2): 219–27. doi:10.1016/j.ijmachtools.2004.07.003.

Lefebvre, Arthur. 1989. *Atomization and Sprays*. New York: Hemisphere Publishing Corp.

Le Gal, P., N. Farrugia, and D. A. Greenhalgh. 1999. "Laser Sheet Dropsizing of Dense Sprays." *Optics & Laser Technology* 31: 75–83.

Linne, Mark, Megan Paciaroni, Tyler Hall, and Terry Parker. 2006. "Ballistic Imaging of the near Field in a Diesel Spray." *Experiments in Fluids* 40 (6): 836–46. doi:10.1007/s00348-006-0122-0.

Lock, James A., and Gérard Gouesbet. 2009. "Generalized Lorenz–Mie Theory and Applications." *Journal of Quantitative Spectroscopy and Radiative Transfer* 110 (11): 800–807. doi:10.1016/j.jqsrt.2008.11.013.

Lozano, A. 1992. "Laser-Excited Luminescent Tracers for Planar Concentration Measurements in Gaseous Jets." PhD Thesis, Stanford University.

Lucht, R. P. 1987. "Applications of Laser-Induced Fluorescence Spectroscopy for Combustion and Plasma Diagnostics." In *Laser Spectroscopy and Its Applications*. Vol. 11. Optical Engineering. New York: Marcel Dekker, Inc.

Meyer, Terrence R., Michael Brear, Seong Ho Jin, and James R. Gord. 2010. "Formation and Diagnostics of Sprays in Combustion." *Handbook of Combustion*. http://onlinelibrary.wiley.com/doi/10.1002/9783527628148.hoc031/full.

Miller, P.C.H, and M.C Butler Ellis. 2000. "Effects of Formulation on Spray Nozzle Performance for Applications from Ground-Based Boom Sprayers." *Crop Protection* 19 (8-10): 609–15. doi:10.1016/S0261-2194(00)00080-6.

Newman, Stephen P. 2005. "Principles of Metered-Dose Inhaler Design." *Respiratory Care* 50 (9): 1177–90.

Nuyttens, D., K. Baetens, M. De Schampheleire, and B. Sonck. 2007. "Effect of Nozzle Type, Size and Pressure on Spray Droplet Characteristics." *Biosystems Engineering* 97 (3): 333–45. doi:10.1016/j.biosystemseng.2007.03.001.

Powell, C. F., Y. Yue, R. Poola, and J. Wang. 2000. "Time-Resolved Measurements of Supersonic Fuel Sprays Using Synchrotron X-Rays." *Journal of Synchrotron Radiation* 7: 356–60.

Ritchie, B., and J. Seitzman. 2002. "Simultaneous Droplet Size and Mixture Fraction Using Acetone PLIF." In . American Institute of Aeronautics and Astronautics. doi:10.2514/6.2002-826.

Schick, Rudolf J. 1997. "General Guidelines on Drop Size Measurement Techniques and Terminology." In *47th Chemical Processing Industry Exposition, NY, November 18*. Vol. 20. http://www.sprayanalysis.com/pdf/compendium_papers/General_03_Schick_CPIE_1997.pdf.

Schulz, Christof, and Volker Sick. 2005. "Tracer-LIF Diagnostics: Quantitative Measurement of Fuel Concentration, Temperature and Fuel/air Ratio in Practical Combustion Systems." *Progress in Energy and Combustion Science* 31 (1): 75–121. doi:10.1016/j.pecs.2004.08.002.

Seitzman, Jerry, and Brian Ritchie. 2004. "Simultaneous Imaging of Vapor and Liquid Spray Concentration Using Combined Acetone Fluorescence and Phosphorescence." In . American Institute of Aeronautics and Astronautics. doi:10.2514/6.2004-384.

Seitzman, J. M., and R. K. Hanson. 1993. "Planar Fluorescence Imaging in Gases." In *Instrumentation for Flows with Combustion*, 405–65. London: Academic Press.

Tate, R. W. 1969. "Sprays." In *Kirk-Othmer Encyclopedia of Chemical Technology*, 2nd ed. Vol. 18. New York: John Wiley & Sons.

Thurber, Mark C., Frédéric Grisch, Brian J. Kirby, Martin Votsmeier, and Ronald K. Hanson. 1998. "Measurements and Modeling of Acetone Laser-Induced Fluorescence with Implications for Temperature-Imaging Diagnostics." *Applied Optics* 37 (21): 4963. doi:10.1364/AO.37.004963.

Thurber, M. C., and Ronald K. Hanson. 1999. "Pressure and Composition Dependences of Acetone Laser-Induced Fluorescence with Excitation at 248, 266, and 308 Nm." *Applied Physics B* 69 (3): 229–40.

Tran, Thao, Yash Kochar, and Jerry Seitzman. 2005. "Measurement of Liquid Acetone Fluorescence and Phosphorescence for Two-Phase Imaging." In . American Institute of Aeronautics and Astronautics. doi:10.2514/6.2005-827.

Trolinger, J. D. 1985. "Particle and Flow Field HolLography: A Critical Survey." Proc. *SPIE* 0532, Holography, 40

Turns, Stephen R. 2012. *An Introduction to Combustion Concepts and Applications*. 3rd ed. New York: McGraw-Hill.

van de Hulst, H. C. 1957. *Light Scattering by Small Particles*. New York: John Wiley & Sons.

Wriedt, Thomas. 2012. "Mie Theory: A Review." In *The Mie Theory*, edited by Wolfram Hergert and Thomas Wriedt, 169:53–71. Berlin, Heidelberg: Springer Berlin Heidelberg. http://link.springer.com/10.1007/978-3-642-28738-1_2.

Yeh, Y, and H. Z. Cummins. 1964. "Localized Fluid Flow Measurements with an He–Ne Laser Spectrometer." *Applied Physics Letters* 4 (10): 176–78.